Study of Supercooled Silicon Liquid-Liquid Critical Point, Structural and Dynamic Properties

A Thesis

Submitted For the Degree of

MASTER OF SCIENCE (ENGINEERING)

in the Faculty of Science

by

Vishwas V Vasisht

THEORETICAL SCIENCES UNIT
JAWAHARLAL NEHRU CENTRE FOR ADVANCED SCIENTIFIC RESEARCH
Bangalore – 560 064

MAY 2009

I dedicate this thesis to my grandparents

Acknowledgements

Well I'm pressing on.. Yes, I'm pressing on.. Well I'm pressing on.. To the higher calling of my Lord. These are the lines from Bob Dylan, an American singer-songwriter. One needs bigger challenges to push oneself. I believe science is one such field where there are plenty of such challenges. I am grateful to my adviser Prof. Srikanth Sastry for providing me an opportunity to be in science and guidance to accomplish and look forward for greater challenges. I am thankful to my lab mates, Shibu, Moumita and Shiladitya for all the help they have been providing me in my research.

I wish to thank all the people who have made this *second innings* at JNCASR a cherishing experience: Prof. Shobhana Narasimhan, Dr. Vidhyadhiraja, Dr. Kavita Jain, Dr. Subir Das, Prof. Swapan Pati, Prof. Umesh Waghmare, Manohar Rao, Dr. Sairam Swaroop, Sreenivas Raju, Surabhi and Gayatri.

I show my gratitude to Dr. Pavan Kumar, Padmanabha, Prabhu, Arathi Harish and Asit Sahoo for backing me to return to the field of science.

I would like to thank most of all, my parents and my brother for their affection and support.

Synopsis

This is a synopsis of the thesis entitled "Study of Supercooled Silicon: Liquid-Liquid Critical Point, Structural and Dynamic Properties", delivered by Vishwas V Vasisht of the Theoretical Sciences Unit, Jawaharlal Nehru Centre for Advanced Scientific Research, Bangalore.

A first order phase transition was shown by Sastry and Angell (Nature Materials, 2, 739, 2003) in supercooled silicon (Stillinger-Weber potential) using computer simulations, from a high density liquid (HDL) to a low density liquid (LDL). In this thesis a detailed and unambiguous simulation evidence is presented for the existence of a liquid-liquid critical point in Stillinger-Weber supercooled silicon. We have taken the approach of constructing the equation of state by performing molecular dynamics simulation and finding the compressibility from the equation of state and from volume fluctuations. We find a van der Waals-like loop below a critical point at negative pressure.

Results from our studies of structural and dynamic properties of the two phases of supercooled silicon are presented. From the radial distribution function calculations the structural properties have been studied as a function of pressure and temperature. We have analysed the local structural

changes using the fifth neighbour distribution and tetrahedrality order parameter. We have calculated the diffusivity of the two phases at different temperature and pressure values and we have found that the diffusivity increases upon compression. This is an anomaly which we observe at all the temperatures we have simulated. We find that there exist a close relation between the coordination number and the diffusivity. We also find a scaling behaviour in temperature for this relation between the coordination number and diffusivity.

In the work on liquid-liquid transition in supercooled silicon, by Sastry and Angell, it was shown that the transition from HDL to LDL also has a characteristic change of behaviour from a fragile to a strong liquid. The fragile behaviour was observed in terms of non-Arrhenius temperature dependence of diffusivity. But the strong liquid identification was based on the existence of a feature in the short time dynamics called the boson peak, which is not universally accepted. We have attempted to provide a clear evidence of strong liquid behaviour by calculating the heat capacity and the diffusivity. Heat capacity was determined from the potential energy fluctuations and has values close to the crystal, leading to very small excess heat capacity, a feature of strong liquids.

Contents

Acknowledgements **i**

Synopsis **ii**

1 Introduction **1**

1.1 Liquid-Liquid Transition in various systems 5

1.1.1 Water 5

1.1.2 Phosphorus 10

1.1.3 Silica 15

1.1.4 Triphenyl phosphite (TPP) 21

1.2 Liquid-Liquid transition in supercooled silicon 22

1.2.1 Analysis of two liquids 24

1.3 Simulation Details 31

1.3.1 Stillinger Weber Potential for Silicon 31

1.3.2 Molecular Dynamics Simulation 39

1.3.3 Other calculations and techniques 44

2 Liquid-liquid critical point in supercooled silicon **47**

2.1 Equation of State 49

2.1.1 Equilibration criteria 50
2.1.2 Relaxation times 57
2.2 Compressibility 62

3 Properties of supercooled silicon 65
3.1 Dynamic properties 66
3.2 Structural properties 68
3.3 Structure and Dynamics 74

4 Low temperature liquid - Strong liquid 76
4.1 Approach 79
4.1.1 Slow Dynamics - MSD and van Hove function 79
4.2 Results 82
4.3 Constrained ensemble Monte Carlo simulation 84

5 Conclusion 87
5.1 Overview 87
5.2 Future work 89

A Appendix 92
A.1 Thermodynamics of phase transitions 92
A.2 Van der Waals equation of state 94
A.3 Radial distribution function and coordination number 98
A.4 Mean square displacement and diffusivity 100
A.5 Density fluctuation, isothermal compressibility and density-density correlation function 103

Bibliography **106**

List of Figures

1.1 Schematic of pressure against temperature plot showing the liquid-gas(L-G) coexistence line, the L-G critical point, the temperature of maximum density (TMD) line and the spinodal. According to stability- limit conjecture, the spinodal intersects the TMD line and the point of intersection spinodal goes through a minima. 6

1.2 Schematic of P-T plot showing the L-G coexistence line, the L-G critical point, the TMD line, the spinodal and HDA-LDA coexistence and critical point. 8

1.3 Plot shows the phase diagram of black phosphorus. The arrows show how melt of black P is obtained for different pressures. Circles represent the low pressure phase and square represent the high pressure phase. The dashed line represent the line of transition [25]. 13

1.4 Left panel: Plot shows the structure factor of liquid phosphorus at different pressures. Right panel: Plot shows the radial distribution function derived from the structure factor [25]. . . 14

1.5 Plot of pressure against temperature for BKS (left panel) and WAC (right panel) silica, for different isochores. Symbols represent the values obtained from MD simulation and the lines are determined from the calculated model equation of state [36]. 16

1.6 Plot of pressure against temperature for BKS (left panel) and WAC (right panel) silica. Plot shows the estimates of the spinodals (solid lines), TMD line (dotted-dashed) and K_T^{max} line (dashed), evaluated from model equation of state [36]. . . 18

1.7 Plot of $g_5(r)$ distribution for BKS (left panel) and WAC (right panel) silica. The arrow indicate the values of cutoff used to identify silicon atoms having high-density coordination or low-density coordination [36]. 19

1.8 Snapshots of MD configurations of BKS (left panel) and WAC (right panel) silica. There are 6000 atoms in each system. Only silicon atoms are shown. Dark spheres are silicon atoms having high-density coordination and light spheres are silicon atoms having low-density coordination. Clustering of atoms with similar coordination into droplets shows the onset of liquid-liquid phase transition [36]. 20

1.9 Plot of enthalpy against temperature from NPH simulations and NPT simulations for the supercooled liquid above and below the liquid-liquid transition. Inset shows the crystal-liquid transition, for comparison with the data in the main panel [37]. 23

1.10 Plot of local bond orientation order parameter distribution (left panel). The continuous line is for the low temperature liquid, which indicates local tetrahedral ordering. Plot of $g_5(r)$ distribution is shown in the right panel. For the case of high temperature liquid (dotted lines), $g_5(r)$ show a uni-modal peak indicating fifth neighbour to be inside the first coordination shell. For the case of low temperature liquid (continuous line), the bimodal peak indicates the expelling of fifth neighbour out of the first coordination shell [37]. 25

1.11 Plot of diffusivity against the inverse temperature above and below the transition. In the high temperature liquid, the diffusivity show a strongly non-Arrhenius temperature dependence [37] 26

1.12 Main panel: The intermediate scattering function F(k,t) from simulation of 512 particles, above and below the transition. The low temperature liquid displays damped oscillatory behaviour, characteristic of strong liquids. The high temperature liquid shows monotonic decrease, characteristic of fragile liquids. Inset: The intermediate scattering function from simulations of a smaller system of 108 particles [37] 28

1.13 Comparison of structure-factor positions in k space (units for k are $\mathring{A}^{-1}$) at $T^* = 0.0817$ [44] 33

1.14 Pair-correlation function for the Si model in crystal phase at $T^* = 0.080$ [44] 34

1.15 Pair-correlation function for the Si model in liquid phase at $T^* = 0.0817$ [44] 34
1.16 (Left panel) Plot of potential energy against MD time step showing the comparison of double sum SW potential implementation with triple loop SW potential implementation. (Right panel) Plot of potential energy calculated from saved configuration of the MD run shows the comparison of double SW potential implementation with triple loop SW potential implementation. Plot shows both the implementations are giving the same values of potential energy. 37
1.17 Plot of potential energy against MD time step and pressures against MD time step showing the comparison of double sum SW potential implementation with the triple loop SW potential implementation. Plot shows the average values of potential energy and pressure remain unaltered. 38

2.1 Plot of potential energy against MD time step. The jump in the value of potential energy indicate that the system has crystallised (at T = 1158 K and P = -1.88 GPa). 51
2.2 Plot of g(r) against distance. An evolution of a small peak is seen between the second and third major peaks, which is an indicator of crystallisation. The green line shows the fully crystallised sample which started from the liquid state and the blue line shows the g(r) for the pure crystal case (at T = 1158 K and P = -1.88 GPa). 53

2.3 Plot of MSD against MD time step for the liquid phase at T = 1259 K and P = 0 GPa. The linear behaviour suggest the system is diffusive. 54

2.4 Plot of potential energy against MD time step shows that the system is yet to equilibrate (at T = 1158 K and P = -1.5 GPa) even after a very long simulation. Each color represent simulation length of 22.5ns. 55

2.5 Plot of MSD against MD time step (right panel) shows that the system is yet to equilibrate (at T = 1158 K and P = -1.5 GPa). Each colour represents a time window of 22.5ns in the trajectory of total time of 92 ns. As the system evolves the diffusivity is changing, which is indicating that the system has not reached its equilibrium state. In the left panel, a small peak in the $g(r)$ evolving between the second and third peak, indicates that the system is crystallising after 40ns of simulation. 56

2.6 Plot of pressure against density -equation of state- for nine different isotherms. The symbols represents the data from NPT simulation. The solid line is the polynomial fit to these data points. The isotherms below $T = 1133K$ are below the critical point and hence a jump in density is observed. 61

2.7 Plot of pressure against density for isotherms which are at or below the critical temperature. The light symbols represent the data from NPT simulation. The dark symbols are data from the NVT simulation. The thick line represents the polynomial fit. 61

2.8 Plot of compressibility against pressure for different temperatures. All these isotherms are below the critical point. With the decrease in temperature the compressibility maxima is increases, suggesting approach to the critical point. The thick line represents the compressibility calculated from the equation of state. The symbols represents the compressibility calculated from the volume fluctuations. 63

3.1 Plot of diffusivity against pressure at different temperatures. Diffusivity decreases with decrease in pressure. 67

3.2 Plot of coordination number against pressure at different temperatures. The coordination number for the HDL phase varies from 4.6 to 5. In the LDL phase the coordination number is around 4.2. 69

3.3 Plot of Radial distribution at different pressures at T = 1259 K. 72

3.4 Plot of Radial distribution at different pressures at T = 1070 K. 72

3.5 Plot of Tetrahedrality order parameter for different temperatures at P = 0 GPa. 73

3.6 Plot of Tetrahedrality order parameter for different pressures at T = 1082 K. 73

3.7 Plot of diffusivity against coordination number at different temperatures. 74

4.1 Plot of viscosity (in log scale) against the scaled temperature (scaling temperature is the glass transition temperature T_g) [3] 78

4.2 Plot of the van Hove function distribution against the MD time function. Inset shows the MSD against the particle displacement ($T = 1070K$ at $P = 0.00GPa$). 80

4.3 Plot of the van Hove function distribution against the MD time function. Inset shows the MSD against the particle displacement ($T = 1057K$ at $P = 0.00GPa$). 81

4.4 Plot of the van Hove function distribution against the MD time function. Inset shows the MSD against the particle displacement ($T = 1052K$ at $P = 0.00GPa$). 81

4.5 Plot of heat capacity against the temperature for high temperature liquid, low temperature liquid and crystal. The orange symbols (with legend SA(2003)) represents the calculation performed by Sastry and Angell. The inset shows the plot for low temperature liquid only. 82

4.6 Plot of diffusivity against the inverse temperature for high temperature liquid, low temperature liquid. The high temperature liquid (black circles) shows non-Arrhenius behaviour in diffusivity, where are the low temperature(red circles) liquid indicates at Arrhenius behaviour. The inset shows the plot for low temperature liquid only. 83

4.7 In the left panel, the cluster growth is shown from a MD run (each configuration number corresponds to a particular MD step). As it can be seen, the threshold cluster size is around 50 in this case. In the right panel, the cluster growth is shown from constrained MC simulation. Here the cluster growth is restricted to a value around50. 85

4.8 Plot of energy against the MC time step from the constrained ensemble simulation. 86

5.1 Plot showing the crystallised run fraction, compressibility and coordination number as a function of pressure 91

A.1 Schematic plot of pressure against volume showing the equation of state obtained from van der Waals equation. 96

Chapter 1

Introduction

First order thermodynamic phase transitions such as solid to liquid and liquid to gas are common phenomena that occur in nature, which include the most common ice to water, water to vapour transformation. Unusual is a transformation between two liquids in a single component system, which is also a first order thermodynamic phase transition. These are called Liquid-Liquid Transitions (LLT). Liquid-liquid transitions have gained considerable focus and interest in recent times. The first section of this chapter gives a brief discussion on some of the important materials which show LLT. A second critical point (first being the Liquid-Gas critical point) associated with LLT was proposed in the context of explanation to thermodynamic anomalies (like the density maxima and the isothermal compressibility minima) observed in the liquid phase of water [35] [explained in the following section]. Even though there are other competing hypothesis explaining the observed anomalies [43] [38], the Liquid-Liquid Critical Point (LLCP) and LLT as a

way of explaining the anomalies has added a new dimension to the rationalisation of such anomalous behaviour. But it should be also noted that in some simulation studies [11] [12] it has been seen that the system do undergo liquid-liquid transition and have a liquid-liquid critical point even in the absence of anomalous behaviour. These studies suggest that the LLT is directly related to certain features of the interaction potential. Even though a complete picture of the origin of LLT is still not clear, the investigation of LLT carried out over a wide range of materials and interaction potentials will be able to answer not only the questions associated with the LLT but also help in better understanding of the liquid phase itself.

A first order phase transition, as in the ice to water or water to vapour cases, involves breaking of bonds and releasing of latent heat, which is evident in the ice-water and water-vapour cases. In the LLT, the underlying principle remains the same. The transition from a high density liquid to a low density liquid shows (in simulations) a non-monotonic behaviour of enthalpy as a function temperature, which lead to an energetically stabilised intermediate density liquid phase, a clear evidence of first order phase transition, as has been shown for silicon [37]. In the LLT not only the density (which is macroscopic quantity), but also the local structure (for example the coordination number) changes with the transition.

In the current work we have studied the liquid-liquid transition and the liquid-liquid critical point in supercooled silicon. Silicon, the second most abundant element on the earth, in its crystalline form is one of the important materials, thanks to its semiconducting nature. In its liquid phase, it shows several intriguing properties [18]. Upon melting, the crystal phase of silicon

transforms from a fourfold semiconducting structure to a metallic higher coordinated liquid. The supercooled phase (liquid phase below the melting point) of silicon has also proved to be as interesting as its other phases. In 2003, Sastry and Angell [37] found that the supercooled liquid silicon undergoes a liquid-liquid transition. Their study also showed some of the interesting structural and dynamic properties of the two liquids. In our work we have carried forward this work on LLT in supercooled silicon to find the critical end point to the liquid-liquid transition. Study of some properties of the supercooled phase of the silicon also have been carried out in the current work. These studies shows that the supercooled silicon phase is a typical network-forming liquid, which shows lots of similarities with other network-forming liquids like water and silica.

The outline of this thesis is as follows. In the first section of the introduction, we discuss, briefly, LLT found in some of the important materials. The second section covers the work of Sastry and Angell [37], which lays the foundation to our current work. In this section we discuss some of results from first principles molecular dynamics studies on supercooled silicon LLT. The third section discusses the model potential used for liquid silicon along with simulation methods and techniques used in our study. In the second chapter we present the work on liquid-liquid critical point in silicon. A detailed discussion of the approach taken to find LLCP is given first, followed by the simulation protocols and results. The work on the LLCP has provided us ample opportunity to study the properties of supercooled silicon, which is discussed in the third chapter. The fourth chapter includes the study of the

low temperature liquid. Sastry and Angell [37] found that the high temperature liquid was a fragile liquid and had predicted that the low temperature liquid would be a strong liquid. We have attempted to provide a conclusive evidence for low temperature liquid to be a strong liquid. In this chapter we discuss the approach and some preliminary results. In the last chapter, after summarising the results of our work, we discuss some of the findings of our current study which needs to be taken up for further investigation.

1.1 Liquid-Liquid Transition in various systems

1.1.1 Water

Liquid-liquid transition and liquid-liquid critical point in the metastable phase of the water was proposed [35] to explain anomalies observed in the liquid phase of water. Prior to this, the origin of anomalies were explained from the 'stability- limit conjecture, which is briefly explained here.

Stability-limit conjecture: A well known equilibrium anomaly in liquid water is the existence of a temperature of maximum density (TMD) at a given pressure. For varying P, we obtain a TMD line (in a P-T plane). The observed TMD line of liquid water, where it has been measured experimentally, has negative slope in the (P,T) plane. A spinodal line represents the limit of stability for a liquid, which lies below the liquid-gas coexistence line in P-T diagram. It has been observed in experiments that this line passes into the negative pressure region. If the trend of TMD line were to continue, without change of slope, it would intersect the spinodal line at negative pressure. But the thermodynamic constraints on the interaction of spinodal and TMD lines demands [43] that the spinodal line pass through a minimum at this intersection point. The spinodal line moves back to higher pressure as the temperature is further lower and eventually becomes positive at sufficiently low temperature (FIG. 1.1). The stability-limit conjecture [43] states that such a re-entrant spinodal actually occurs in liquid water and it is responsible for the anomalous behaviour of the liquid at low temperature.

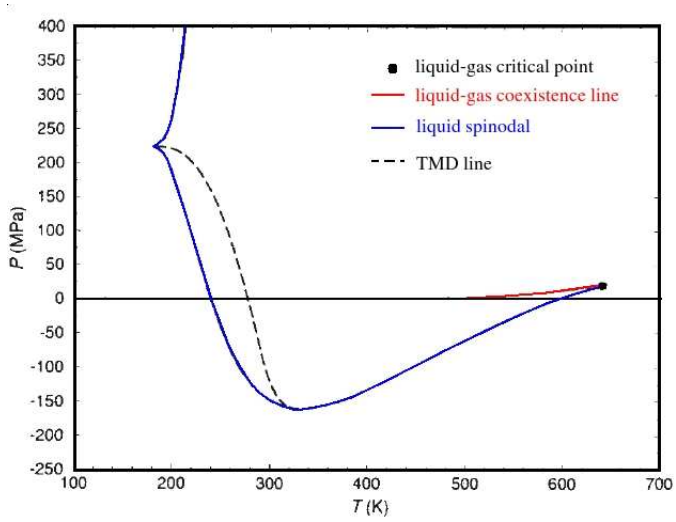

Figure 1.1: Schematic of pressure against temperature plot showing the liquid-gas(L-G) coexistence line, the L-G critical point, the temperature of maximum density (TMD) line and the spinodal. According to stability- limit conjecture, the spinodal intersects the TMD line and the point of intersection spinodal goes through a minima.

Second critical point scenario: Results from molecular dynamics simulations conducted by Poole and co-workers [35] on ST2 potential water suggested something which is very different from what is shown in the FIG. 1.1. The scenario suggested by their results is given in FIG. 1.2. In their simulation the spinodal line was obtained from calculating the isothermal compressibility ($K_T = -\frac{1}{V}\frac{\partial V}{\partial P}_T$). The state point in the (P,V) plane where the compressibility becomes singular gives the limit of stability. The results from the their simulations are as follows:

1. The spinodal is a monotonic function of T and there is no re-entrace.

2. The TMD line although has negative slope at high pressure, it acquires a positive slope at low pressure (FIG. 1.2).

Hence there is no intersection between the spinodal and the TMD line, as suggest by the stability-limit conjecture.

Their investigation suggested instead of an intersection, a novel critical point, which was not related to the liquid-gas critical point (FIG. 1.2). The evidence that backed the second critical point are as follows:

1. In the (P,V) diagram, they found at the low temperatures around $\rho = 1.00 gcm^{-3}$, an inflection develops. This is a trend similar to what would occur for isotherms, if the critical point were to be approached from above in temperature.

2. Onset of a two phase coexistence region below the critical point was explored by looking at the pair-correlation function $g(r)$ and matching

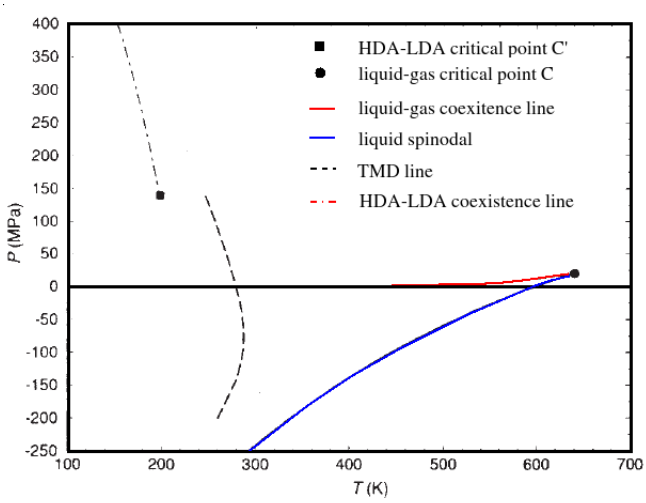

Figure 1.2: Schematic of P-T plot showing the L-G coexistence line, the L-G critical point, the TMD line, the spinodal and HDA-LDA coexistence and critical point.

with the $g(r)$ obtained from experiments for the HDA (High Density Amorphous) and LDA (Low Density Amorphous) phases.

Even though this and other simulation results (See Ref. [31]) have predicted the LLT in water, the experimental realisation has been difficult to achieve. Access to the temperature regime below the homogeneous nucleation temperature (T_H) is hard as the water crystallises spontaneously. In 1998, Mishima and Stanley reported [31] an experimental approach which is not restricted by the barrier imposed by T_H. They found melting curve of ice IV to undergo a discontinuity at the location proposed for the line of liquid-liquid phase transitions. They also reported the finding of liquid-liquid critical point.

Singularity-Free interpretation: In this interpretation, by Sastry and

co-workers [38], the retracing of TMD is shown even in the absence of spinodal retracing. Locus of compressibility extrema in (P,T) plane, called the Temperature of Extremal Compressibility or TEC is shown to be playing a significant role in the analysis. It is associated with the retracing TMD. They find in a water-like lattice model simulation, TEC intersects the TMD with positive slope and the spinodal in the system is not retracing. Thermodynamic arguments are given to show that if an anomalous liquid exhibits a negatively sloped TMD, then the isothermal compressibility at constant pressure increases on decreasing temperature and hence the increases in compressibility are not *a priori* an indication of a singular behaviour. Their arguments also show that when the liquid does not exhibit a retracing spinodal, the TMD retraces to lower temperature upon intersecting with the locus compressibility extrema. In this scenario, generally the resulting phase diagram exhibits a locus of compressibility maxima along isobars. Hence in the simplest interpretation of simulation data for supercooled water one expects a line of compressibility maxima at low temperatures. The metastable critical point scenario, from these arguments, seems to be a special case where the compressibility at points of TEC locus either diverges (at the critical point) or discontinuous (at the first order line). Alternatively, it has been argued that the singularity free scenario is a limiting case where the critical point moves to zero T [13].

1.1.2 Phosphorus

The element phosphorus shows a number of allotropes in the solid state. White P consists of tetrahedral molecules, whereas black P is a layered structure and red P is usually amorphous. Each allotrope has a different melting temperature. White P melts at 44° while black P and red P melt at around 600°. In the black P allotrope, Katayama and co-workers found a first order liquid-liquid phase transition [25]. They studied the structure of the melt of black P by an *in situ* X-ray diffraction method. The results and analysis of their work is briefly discussed in this subsection.

In FIG. 1.3, the phase diagram black P [2], is shown. Katayama and co-workers, conducted X-ray diffraction experiment at several pressures in the melt of black P (represented by symbols in the FIG. 1.3. The arrows in FIG. 1.3 shows how they obtained the black P melt at different pressure. In FIG. 1.3, the circles represent the low pressure phase and the squares represent the high pressure phase. From the analysis of the structure factor and the radial distribution function they show there exists a phase transition between these two phases.

Structure Factor: FIG. 1.4 shows the structure factor, $S(Q)$, at four different pressures, as obtained by the authors, from X-ray diffraction data. A large difference in $S(Q)$ was observed below and above $1GPa$. At around 1.4Å^{-1}, for the case of low pressure, a prominent peak was observed, which disappeared at high pressures and a new maxima was found to appear at around 2.45Å^{-1}. The $S(Q)$ observed at $0.77GPa$ and $0.96GPa$ were found

to be identical and the $S(Q)$ observed at $1.01GPa$ was similar to the $S(Q)$ at $1.38GPa$. From these results the authors found an indicator towards the existence of two distinct forms of liquid (which they call low-pressure and high-pressure form). The $S(Q)$ for the melt of white P at 50° and the $S(Q)$ for the low pressure were found to resemble each other. In the case of melt of white P, the prominent first peak at around 1.5Å^{-1} has been attributed to correlation between the P_4 molecules. Hence the authors conclude, it is highly probable that the low-pressure form should be a molecular liquid. The small first peak at 1.25Å^{-1} in the high-pressure form is different from that in the low-pressure form. They further analyse the radial distribution function obtained from the $S(Q)$ to find the local atomic structure.

Radial distribution function $g(r)$: FIG. 1.4 shows the $g(r)$ which the authors derived from $S(Q)$. Since there were no density data available for liquid P under high pressure, the authors have tentatively taken the densities to be $2.0gcm^{-3}$ for the low-pressure form and $2.8gcm^{-3}$ for the high-pressure form, in order to calculate the $g(r)$. Owing to these uncertainties, the authors restrict the observation from $g(r)$ to peak positions and relative peak intensities. In the $g(r)$ for the low-pressure form, a sharp peak with a maxima at 2.22Å was observed. The authors find this position to be in good agreement with the P-P distance in P_4 molecules in the melt of white P. The intensity in the second-neighbour region (2.5 to 4.5Å) was found to be low and the third peak around 5.5Å was found to be broad. All these supported a picture in which the low pressure form comprises of P_4 molecules without strong bonds between them. Hence the authors conclude low pressure form is a molecular liquid. In the high-pressure form, the g(r) was found to be showing a very

different feature. The appearance of a distinct second peak around 3.5Å was found. The strong correlation between the second-nearest neighbours is not consistent with the nature of molecular liquid, where the molecular interaction become weak as one move away from the first coordination shell. The authors think of a possibility of a polymeric liquid in which P atoms form network structures. From the comparison of the $g(r)$ of the high pressure form with $g(r)$ of the red amorphous P, which has a polymeric nature, the authors conclude, it is very likely that the high-pressure liquid is a polymeric liquid. The authors could also reproduce diffraction pattern taken during the transformation from the diffraction pattern taken before and after the transformation. All these observation supported the view that the transition is a first-order liquid-liquid phase transition from molecular liquid to polymeric liquid. These observations have also been supported independently by computer simulations [33] [5]. In 2003, experiments conducted by Monaco and co-workers [32] gave a clear evidence of the first order phase transition in terms of change in latent heat.

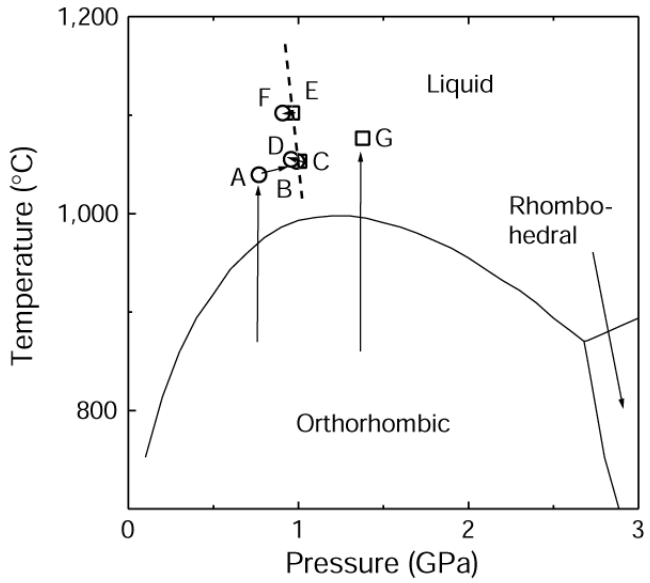

Figure 1.3: Plot shows the phase diagram of black phosphorus. The arrows show how melt of black P is obtained for different pressures. Circles represent the low pressure phase and square represent the high pressure phase. The dashed line represent the line of transition [25].

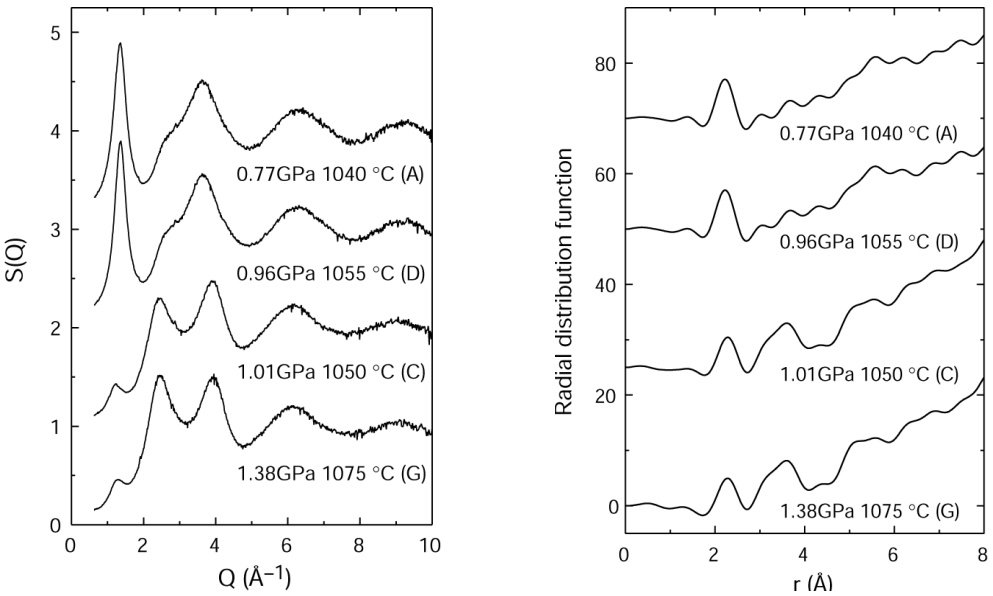

Figure 1.4: Left panel: Plot shows the structure factor of liquid phosphorus at different pressures. Right panel: Plot shows the radial distribution function derived from the structure factor [25].

1.1.3 Silica

Silica, a substance structurally similar to water also shows Liquid-liquid phase transition. It was found, using simulation, by Saika-Voivod and co-workers [36] in two different model potential of silica (BKS and WAC model potentials). Rosenfeld and Tarazona had predicted [47] that in a simple dense liquid at low temperature, the isochoric T dependence of the potential energy U is given by $U = a + bT^{3/5}$. In the work of Saika-Voivod and co-workers on silica, the authors first identify a region of validity (in T and V) where in the above dependence of potential energy U is obeyed. To start with the authors obtained the functional representation of U in terms of a(V) and b(V), where a(V) $\simeq \sum_{n=0}^{4} \alpha_n V^n$ and b(V) $\simeq \sum_{n=0}^{4} \beta_n V^n$. The internal energy is E = U + U_k, where for classical ionic models of silica, the kinetic energy $U_k = \frac{9}{2}RT$, R being the gas constant. Hence,

$$E(V,T) = a(V) + b(V)T^{3/5} + \frac{9}{2}RT$$

Next, a functional representation of the entropy was calculated, so that a model for A(V,T) can be obtained from A = E - TS. Here S at arbitrary V and T, relative to the entropy of a reference state ($S(V_o, T_o)$) was evaluated by thermodynamic integration. This was done in two steps, first along an isotherm and then along an isochore. The combined contribution is given by

$$S(V,T) = S(V_0,T_0) + \Delta S_T + \Delta S_V$$

where ΔS_T was computed along an isotherm and ΔS_V was computed along an isochore.

Using the model functions for E and S, A(V,T) was obtained and hence the equation of state

$$P(V,T) = -\left(\frac{\partial A}{\partial V}\right)_T$$

To summarise, the model P(V,T) equation of state was constructed using as input, polynomial fits of (i) the V dependence of a and b and (ii) one reference isotherm of P. The calculated and simulated equation of state was compared as a check (FIG. 1.5).

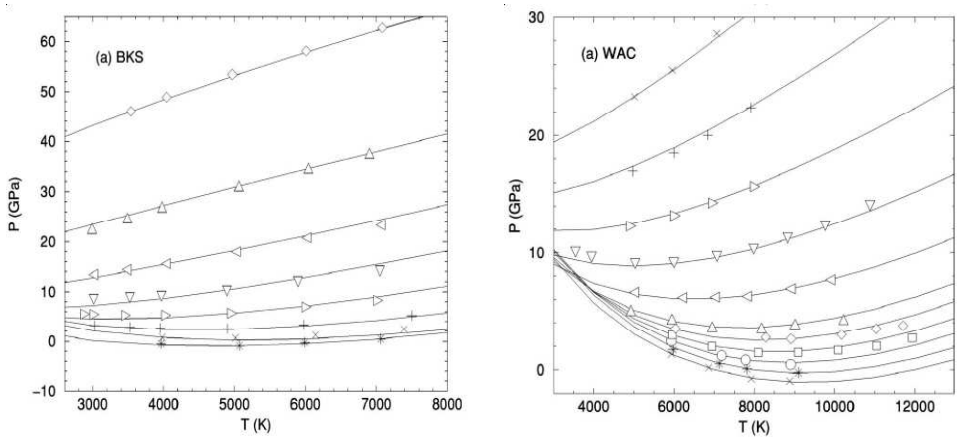

Figure 1.5: Plot of pressure against temperature for BKS (left panel) and WAC (right panel) silica, for different isochores. Symbols represent the values obtained from MD simulation and the lines are determined from the calculated model equation of state [36].

Following three thermodynamic conditions were evaluated from the model equation of state:

1. Along the TMD (Temperature of Maximum Density) line, the condition

$$\left(\frac{\partial P}{\partial T}\right)_V = 0$$

is satisfied.

2. The metastability limit of the liquid, or spinodal line, is defined by

$$\left(\frac{\partial P}{\partial V}\right)_T = 0$$

3. Along the K_T^{max} line, the isothermal compressibility K_T is a maximum with respect to V at constant T. It is found by locating points satisfying

$$\left(\frac{\partial K_T}{\partial V}\right)_T = 0$$

and then checked to confirm that the extremum so identified is a maximum. The occurance of a K_T^{max} line is a necessary, but not a sufficient condition for the occurance of a critical point [38]. Note that K_T^{max} line differs from that of the temperature of extermal compressibility defined in [38]. (Authors in this paper state that it is simpler to identify the K_T^{max} line in an isothermal compression experiment).

The locations of these lines are shown in FIG. 1.6 projected onto the P-T plane. The pattern of behaviour was found to be same, quantitatively, for both WAC and BKS silica. Also these pattern were similar to one found in water simulations. At the low temperature regime, in both the model potentials, as spinodal line is observed, which is distinct from the liquid-gas

spinodal boundary. This spinodal is the metastability boundary associated with a liquid-liquid phase transition. The critical point of this liquid-liquid transition should occur at the point of the maximum temperature on the spinodal line.

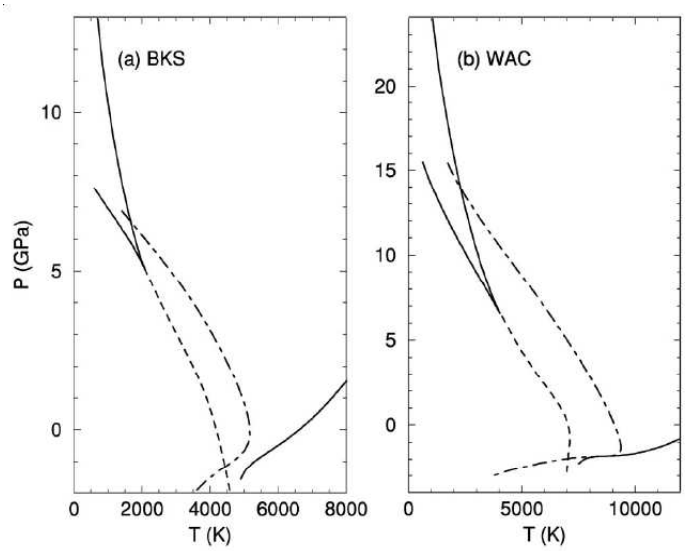

Figure 1.6: Plot of pressure against temperature for BKS (left panel) and WAC (right panel) silica. Plot shows the estimates of the spinodals (solid lines), TMD line (dotted-dashed) and K_T^{max} line (dashed), evaluated from model equation of state [36].

If the spinodal curves predicted by the equations of state are correct, equilibrium simulations in these regions should give characteristic signs of phase separation. The local coordination environment of silicon atoms were examined to test the occurrences of such a phase separation. The fifth neighbour distribution calculated at different temperatures along the isochores are shown in FIG. 1.7. It was observed, for T above the T_C $g_5(r)$ distribution

was unimodal function of r and as T decreases width of the distribution increases. For temperature near T_C, the distribution becomes bimodal, which indicates, two distinct 5^{th} nearest neighbour coordination environments are emerging.

Spatial correlation in Si atoms with similar coordination environment were analysed by performing bigger system simulation (6000 atoms). The spatial correlation were found by examining the snapshots of the configuration (FIG. 1.8).

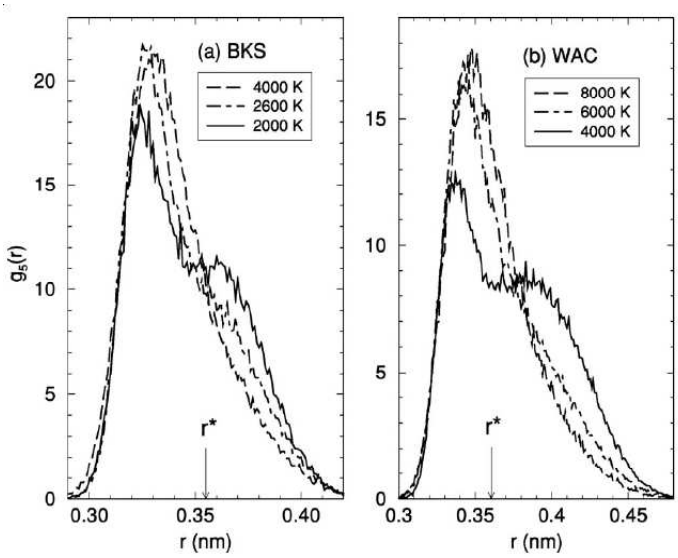

Figure 1.7: Plot of $g_5(r)$ distribution for BKS (left panel) and WAC (right panel) silica. The arrow indicate the values of cutoff used to identify silicon atoms having high-density coordination or low-density coordination [36].

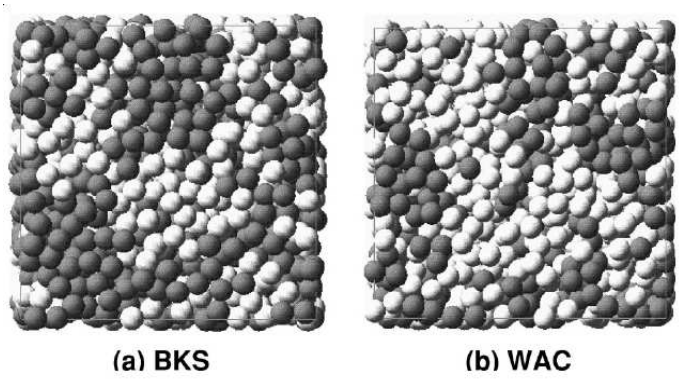

Figure 1.8: Snapshots of MD configurations of BKS (left panel) and WAC (right panel) silica. There are 6000 atoms in each system. Only silicon atoms are shown. Dark spheres are silicon atoms having high-density coordination and light spheres are silicon atoms having low-density coordination. Clustering of atoms with similar coordination into droplets shows the onset of liquid-liquid phase transition [36].

1.1.4 Triphenyl phosphite (TPP)

An unusual phenomena found by Kivelson and co-workers led to the finding of LLT in TPP by Tanaka and co-workers. Kivelson and co-workers found, when TPP is cooled rapidly enough, it first enters the supercooled liquid state below the melting point T_M $(295K)$ as usual liquids and then into a glassy state at the glass-transition temperature T_g^I $(205K)$ called glass I. This supercooled liquid (liquid I) behaves as a typical fragile glass former. On the other hand, if TPP is quenched to a certain temperature between $210K$ and $223K$ (above T_g^I) and then annealed at that temperature, a new phase emerged in a supercooled liquid. This phase were termed as the glacial phase. Many explanation were given to the nature and origin of this glacial phase, which included, exotic defect-ordered phase to plastic crystal. Tanaka and co-workers, in 2004, gave an experimental evidence which indicates that the TPP undergoes a liquid-liquid transition [45] and that the glacial phase is the glassy state of the second liquid (liquid II). Even though this is still a matter of active debate, progress has been done by Tanaka's group to show not only LLP in TPP, but also critical-like phenomena associated with this [28]. Recently an application related to LLT in TPP has has also been shown [46] by their group. They report that they can control, by the LLT of TPP, the fluidity and miscibility of its mixture with another molecular liquid (toluene or aniline).

Liquid-liquid transition has been found in many more materials either in simulation or in experiments. These include $Al_2O_3Y_2O_3$ [1], Carbon [16],

Molten Silicates [26], Heavy Water [30], Compressed Hydrogen [39]. LLT has been also found in model potentials which resembles potentials used in colloids and proteins [41].

From the previous section discussions, we infer the wide ranged importance of the field of liquid-liquid transition. The field has caught attention not only because of its fundamental importance but also, as for its applications [27]. In the next section we discuss in detail the work of Sastry and Angell on liquid-liquid transition in supercooled silicon.

1.2 Liquid-Liquid transition in supercooled silicon

Simulation evidence that showed a first order phase transition in supercooled liquid silicon (using Stillinger-Weber potential) from a High Density Liquid (HDL) to a Low Density Liquid (LDL), was provided by Sastry and Angell [37]. In their work, the authors found considerable change in the structure as the liquid undergoes transition. They also reported that the transition marks a change in liquid's dynamic character from that of a fragile liquid to a strong liquid.

To probe whether a first-order transition exists, the authors carried out constant enthalpy (NPH) simulations. A non-monotonic dependence of the enthalpy on temperature was found (FIG. 1.9), which is indicative of a phase transition. The transition was found to be at $T = 1060K$ at zero pressure.

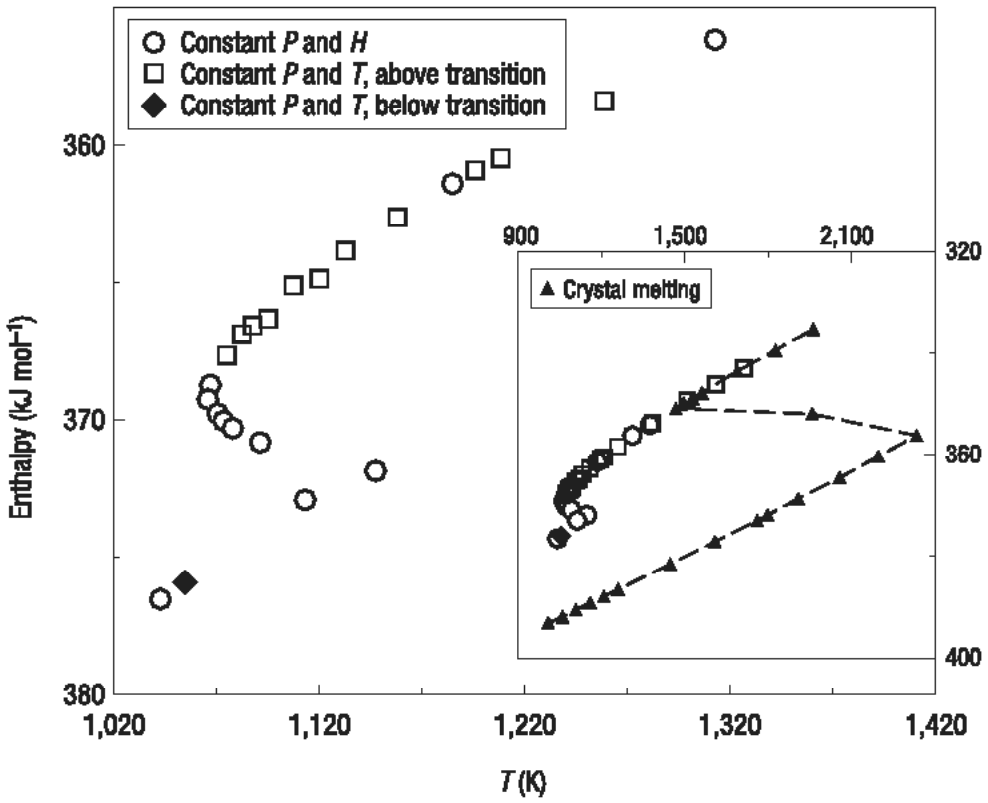

Figure 1.9: Plot of enthalpy against temperature from NPH simulations and NPT simulations for the supercooled liquid above and below the liquid-liquid transition. Inset shows the crystal-liquid transition, for comparison with the data in the main panel [37].

1.2.1 Analysis of two liquids

Structural analysis

Structural studies were carried out from calculations of the pair correlation function $g(r)$, the fifth neighbour distribution $g_5(r)$, the bond angle correlation function G_3 and the local bond orientation order parameter Q_3. From $g(r)$, the coordination number was calculated and it was found that the average coordination number changes from 5.12 to 4.61 in the high-temperature liquid and jumps to a value of around 4.2 in the low-temperature liquid. The fraction of four- coordinated atoms jumps from about 50% to 80% indicating that below the transition the liquid has a greater degree of local tetrahedral order. The local bond orientation order Q_3 gives the distribution of local bond ordering. The low temperature liquid's Q_3 values sharply peak near the perfect crystal's Q_3 value, suggesting that the low temperature liquid to be a having a tetrahedral local ordering. The high temperature liquid shows a broader peak in Q_3. From the fifth neighbour distribution it was found that in the high temperature liquid, the first coordination shell contains five neighbour (indicated in $g_5(r)$ as uni-modal peak), whereas in the low temperature liquid, the fifth neighbour is expelled out of first coordination shell (indicated in $g_5(r)$ as bimodal peak). FIG. 1.10 shows the Q_3 and $g_5(r)$ distributions.

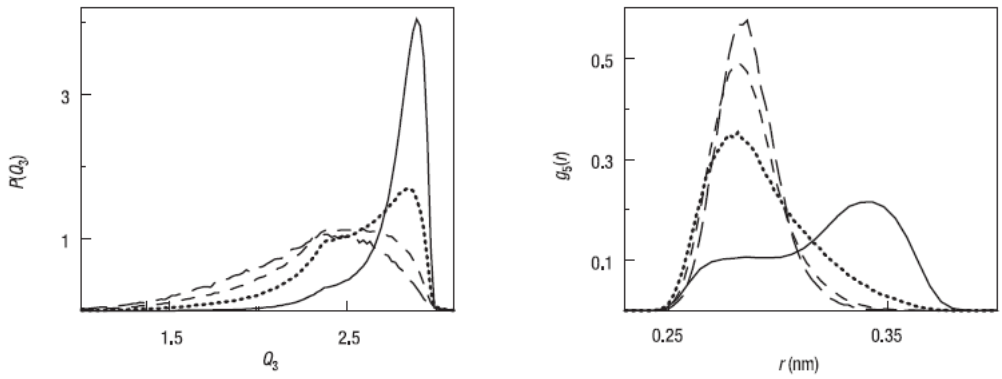

Figure 1.10: Plot of local bond orientation order parameter distribution (left panel). The continuous line is for the low temperature liquid, which indicates local tetrahedral ordering. Plot of $g_5(r)$ distribution is shown in the right panel. For the case of high temperature liquid (dotted lines), $g_5(r)$ show a uni-modal peak indicating fifth neighbour to be inside the first coordination shell. For the case of low temperature liquid (continuous line), the bimodal peak indicates the expelling of fifth neighbour out of the first coordination shell [37].

Analysis of Dynamic property

To study the dynamics, diffusivity at various temperatures were calculated from mean square displacement (MSD). The diffusivity dropped roughly by two orders of magnitude with the transition from one liquid phase to other. The high temperature liquid dynamics was found to be faster than the low temperature (LDL) liquid dynamics. The FIG. 1.11 shows the change in diffusivity as a function of inverse temperature. It was observed that the high temperature liquid phase (about $T = 1070K$) the T-dependence of the diffusivity is highly non-Arrhenius. This is a characteristic of a fragile liquid.

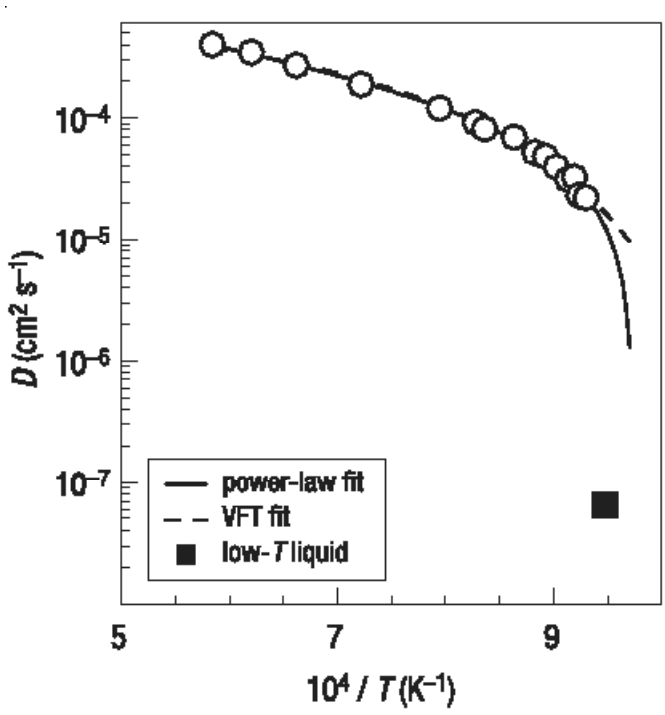

Figure 1.11: Plot of diffusivity against the inverse temperature above and below the transition. In the high temperature liquid, the diffusivity show a strongly non-Arrhenius temperature dependence [37]

The dynamical behaviour of the low temperature phase was addressed in an indirect way, by studying the boson peak, a feature in the short time dynamics. It is commonly observed in the laboratory that strong liquids show strong boson peaks [42]. In simulation studies the boson peak has been identified [17] as a dip in the intermediate scattering function between the short time process and the caging plateau that precedes the alpha relaxation. The intermediate scattering function $F(k,t)$ for $T = 1070K$ and $T = 1055K$ is shown in FIG. 1.12. The $F(k,t)$ plot shows oscillatory behaviour that is seen only in low temperature liquid. This provided a supporting evidence for fragile to strong transition. Same data for smaller system size of 108 particles shows a finite size effect, which disappears in fragile liquid.

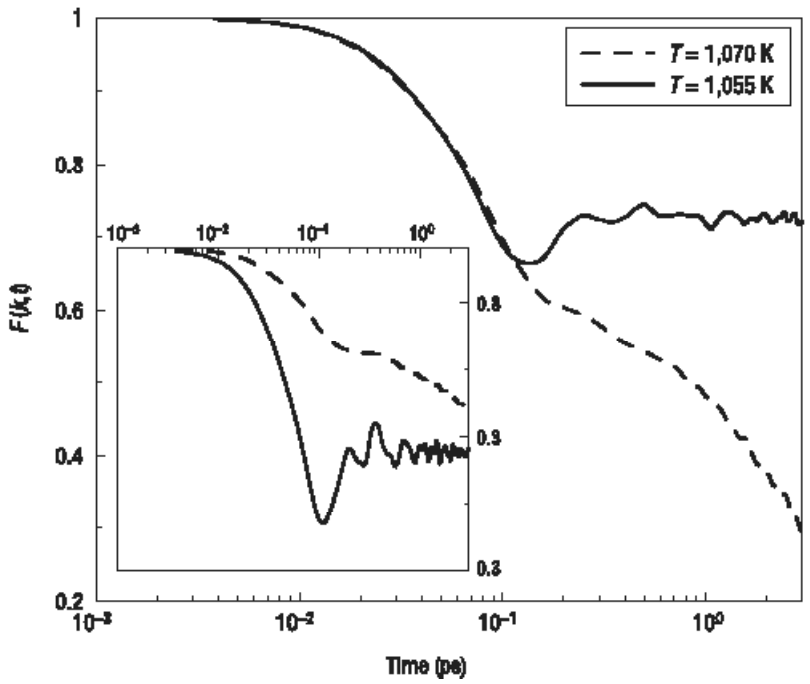

Figure 1.12: Main panel: The intermediate scattering function F(k,t) from simulation of 512 particles, above and below the transition. The low temperature liquid displays damped oscillatory behaviour, characteristic of strong liquids. The high temperature liquid shows monotonic decrease, characteristic of fragile liquids. Inset: The intermediate scattering function from simulations of a smaller system of 108 particles [37]

First principles study of supercooled silicon: In 2007, Jakse and Pasturel used the method of first-principle molecular dynamics (FPMD) to study the liquid-liquid phase transformation in silicon [21]. The approach was similar to the one followed by Sastry and Angell. They did NPH simulation and found that the enthalpy decrease monotonically till $T = 1050K$. A further decrease of enthalpy induced a rise of the temperature indicating a first order phase transition. The time span of the FPMD simulation was $25ps$ at $T = 1070K$, the HDL phase and $42ps$ at $T = 1050K$, the LDL phase. They find that the coordination number for the HDL phase is around 4.36 and for the LDL phase is around 4.08. There is a discrepancy in the values of coordination number they have obtained and from those obtained from SW potential MD simulations (HDL - 5.2 to 4.6 and LDL - 4.2). They believe that the reason behind this is the difficulty of empirical potentials to describe the changes in chemical bonds induced by the density and temperature variations [20].

In 2009, another study on supercooled silicon was done by Ganesh and Widom using the first principles molecular dynamics method [15]. They report the finding of a liquid-liquid critical point. They have performed NVT simulations between $T = 982K$ and $T = 1382K$. At each temperature and volume the simulation spanned around $5ps$. They have reported the finding of van der Walls loops below the critical point, indicating the phase transition. They find that the coordination number changes from 5.6 in the HDL phase to 4.2 in the LDL phase, which is more consistent with the SW potential simulation than the FPMD simulation from Jakse and Pasturel [21].

A point to note is that the simulation time in both the works based on

FPMD is of the order of pico seconds and both the works do not report the details of equilibration in the system. Another observation is that even though both are FPMD based calculation there is a discrepancy in coordination numbers found. A better comparative study of SW potential based simulations and FPMD based simulation needs to be carried to know the limitations of both the methods. In our work we find that the LDL requires tens of nano seconds to equilibrate. We also find that the coordination number is playing a prime role in the dynamics of the system. In HDL the coordination number is around five and the relaxation times are around tens of picoseconds. In LDL the coordination number is nearing four and the relaxation times increases to nano second regime. We believe even if we include the correction to SW potential, as suggested by Jakse and co-workers [20], the coordination number will not change more than 5% from what we have found from our simulations and hence the relaxation times of the LDL phase should be having the same order of magnitude as we have found.

We discuss in the next section details of the model potential used for liquid silicon and simulation methods.

1.3 Simulation Details

1.3.1 Stillinger Weber Potential for Silicon

Stillinger Weber potential is one of the most widely used model potential for simulations of liquid silicon. It was approximated [44] as a combination of a pair (v_2) and a triplet potential (v_3), keeping in mind that the Si crystal consists of atoms held in place by strong and directional bonds.

The pair potential part (v_2) was selected so as to make the cutoff at r = a, without discontinuities in any r derivatives, which is a distinct advantage in molecular dynamics simulations. The form of v_2 is given by

$$v_2(r_{ij}) = \epsilon f_2(r_{ij}/\sigma) \tag{1.1}$$

where

$$f_2(r_{ij}) = \begin{cases} A(Br^{-p} - r^{-q}exp[(r-a)^{-1}] & \text{if r<a} \\ 0 & \text{if r}\geq\text{a} \end{cases} \tag{1.2}$$

The same cutoff advantage is extended to the three body interactions, which is given by

$$v_3(\vec{r}_i, \vec{r}_j, \vec{r}_k) = \epsilon f_3(\vec{r}_i/\sigma, \vec{r}_j/\sigma, \vec{r}_k/\sigma) \tag{1.3}$$

where

$$f_3(\vec{r}_i, \vec{r}_j, \vec{r}_k) = h(r_{ij}, r_{ik}, \theta_{jik}) + h(r_{ji}, r_{jk}, \theta_{ijk}) + h(r_{ki}, r_{kj}, \theta_{ikj}) \tag{1.4}$$

Here, θ_{jik} is the angle between $\vec{r}_j$ and $\vec{r}_k$ subtended at the vertex i, etc.

Functional form of h is given by

$$h(r_{ij}, r_{ik}, \theta_{jik}) = \lambda exp[\gamma(r_{ij} - a)^{-1} + \gamma(r_{ik} - a)^{-1}] \times (cos\theta_{jik} + \frac{1}{3})^2 \quad (1.5)$$

In obtaining the values for the seven parameters A, B, p, q, a, λ and γ, it was ensured that the diamond structure was indeed the most stable periodic arrangement of particles at low pressure. Along with this criteria, the chosen values for these parameters should also give correct melting point and liquid structure (in reasonable accord with experiment). Satisfying these three criteria, the following set of parameters were found.

$$A = 7.049556277, B = 0.6022245583, p = 4, q = 0, a = 1.80, \lambda = 21.0, \gamma = 1.20 \quad (1.6)$$

To test the potential, the authors performed molecular dynamics simulations and obtained the following results.

1. The melting temperature was estimated to be $T_m \cong 1691K$ is in good agreement with the experimental melting temperature ($1687K$).

2. The entropy change that accompany the transition from crystal to liquid was found to be $\Delta S/Nk_B \cong 3.7$. The experimental melting value at 1 atm is $\Delta S(expt)/k_B = 3.25$.

3. Local ordering was analysed by looking at the RDF g(r) and structure factor S(k) in both, crystal and liquid phase. The crystal g(r) showed

highly structured organisation of atoms. The coordination number obtained from g(r) shows four nearest neighbours, as in the case of diamond crystal. The second and higher order coordination shells have their positions and magnitude to be as expected for a vibrating but structurally perfect diamond lattice.

The liquid phase g(r) in comparison with the crystal, shows drastic structural change that occurs at melting. The g(r) shows broader and considerably lower first peak. The gap between the first and second coordination shell as seen in the crystal disappears. FIG. 1.14 and 1.15 shows the g(r) calculated by the authors [44] from the molecular dynamics simulation.

4. The structure factor S(k) for liquid phase was in comparison with those from the diffraction experiments on molten Si. FIG. 1.13 gives the simulation and experimental comparison of structure factor positions in k space at $T^* = 0.0817$.

Feature	Molecular dynamics	Experiment
First peak	2.53	2.80
Shoulder	3.25	3.25
Second peak	5.35	5.75
Third peak	8.16	8.50
Fourth peak	10.60	11.20

Figure 1.13: Comparison of structure-factor positions in k space (units for k are $\mathring{A}^{-1}$) at $T^* = 0.0817$ [44]

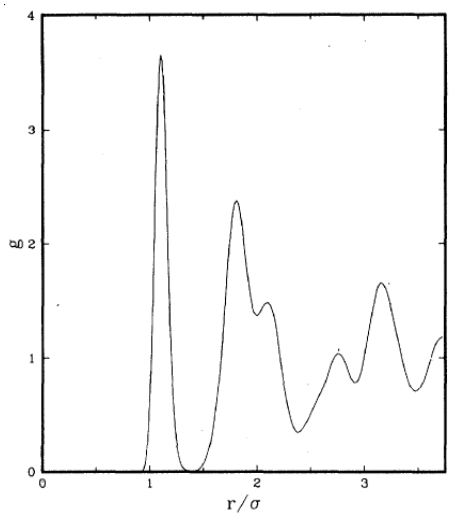

Figure 1.14: Pair-correlation function for the Si model in crystal phase at $T^* = 0.080$ [44]

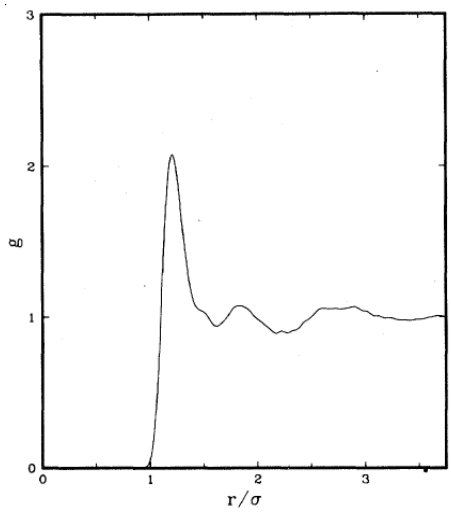

Figure 1.15: Pair-correlation function for the Si model in liquid phase at $T^* = 0.0817$ [44]

All our simulation results discussed in this work has been performed using this potential. Since this potential includes a three body term, it is computationally expensive (as compared to pair potential models). A novel algorithm, which uses two body sums to calculate the three body term was developed by Makhov and Lewis [29]. In their work, the three body potential was re-written in terms of a double sum, as explained below.

The Stillinger-Weber potential is given by

$$U = \sum_{r_{ij}<a} v_2(r_{ij}) + \sum_{r_{ij},r_{ik}<a} \frac{1}{2}\phi(r_{ij}, r_{ik}) \tag{1.7}$$

where

$$v_2(r_{ij}) = \epsilon A(Br_{ij}^{-4} - 1)exp(\frac{1}{r_{ij} - a}) \tag{1.8}$$

$$\phi(r_{ij}, r_{ik}) = \lambda exp(\frac{\gamma}{r_{ij} - a} + \frac{\gamma}{r_{ik} - a})(cos\theta_{jik} + \frac{1}{3})^2 \tag{1.9}$$

which is re-written as

$$U = \sum_i \sum_{j<i} v_{ij}^{eff} + \sum_i U_i^d \tag{1.10}$$

where

$$v_{ij}^{eff} = v_2(r_{ij}) - \frac{16\lambda}{9} g_{ij}^2 \tag{1.11}$$

and

$$U_i^d = \frac{\lambda}{18} h_i^2 + \frac{\lambda}{3}|\mathbf{s}_i^2| + \frac{\lambda}{2} Tr[\mathbf{T}_i]^2 \tag{1.12}$$

Here h_i is a scalar, $\mathbf{s}_i$ is a vector and $\mathbf{T}_i$ is a matrix, which are defined as

$$h_i = \sum_i g_{ij}, \text{ where } g_{ij} = exp[\gamma/(r_{ij} - a)] \tag{1.13}$$

$$\mathbf{s}_i = \sum_j g_{ij}\hat{\mathbf{r}}_{ij} \tag{1.14}$$

and

$$\mathbf{T}_i = \sum_{j \neq i} g_{ij}(\hat{\mathbf{r}}_{ij} \otimes \hat{\mathbf{r}}_{ij}) \tag{1.15}$$

Makhov and Lewis in their work did Monte Carlo simulation and hence they did not describe the calculation of forces. Niels Ellegaard [9] extended this work and did the calculation of forces, which has been used in our implementation of MD simulation.

We implemented the new algorithm and compared the energy and the pressure obtained from the new algorithm with that of the simple (triple loop) implementation of SW potential. The energy and pressure values match exactly (up to 14 decimal points) in the initial MD steps. At the later part of the simulation, the errors in the least significant digit add up to give a noticeable difference in the energy and pressure calculated from the two codes (FIG. 1.16). But the averages remain unaltered (FIG. 1.17). We also calculated the energy from saved configuration (around 14000) from the previous runs. This way, we can eliminate the issue of adding of errors and can confirm the new algorithm implementation is giving the correct results (FIG. 1.16).

All the results in this work is obtained using this implementation. This

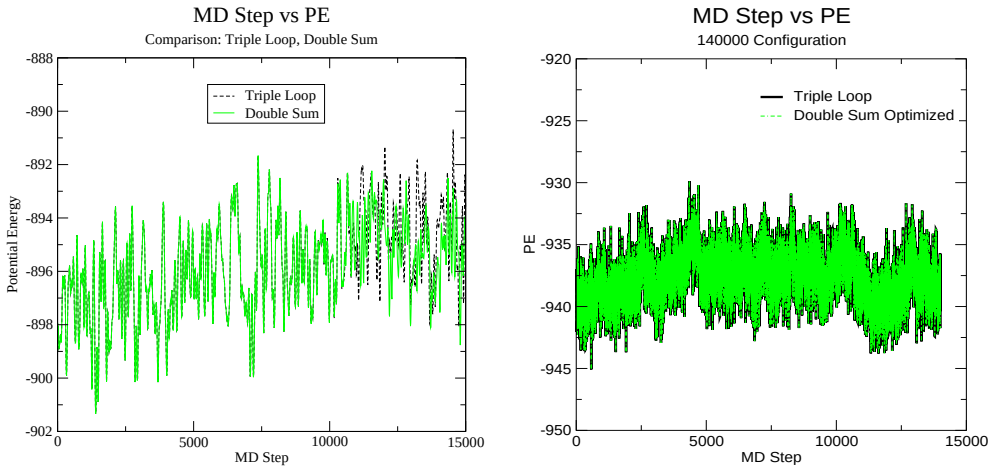

Figure 1.16: (Left panel) Plot of potential energy against MD time step showing the comparison of double sum SW potential implementation with triple loop SW potential implementation. (Right panel) Plot of potential energy calculated from saved configuration of the MD run shows the comparison of double SW potential implementation with triple loop SW potential implementation. Plot shows both the implementations are giving the same values of potential energy.

implementation is around 6 times faster than the triple loop implementation of SW potential.

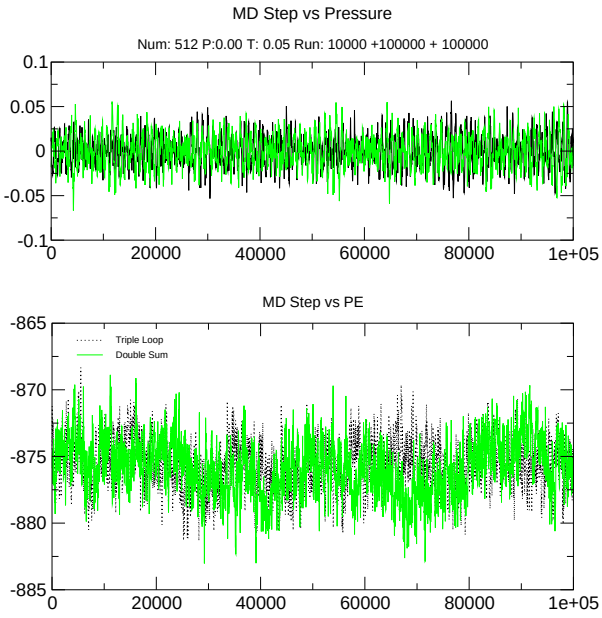

Figure 1.17: Plot of potential energy against MD time step and pressures against MD time step showing the comparison of double sum SW potential implementation with the triple loop SW potential implementation. Plot shows the average values of potential energy and pressure remain unaltered.

1.3.2 Molecular Dynamics Simulation

Molecular dynamics simulation is a technique for computing the equilibrium and transport properties of a classical many-body system. These simulations are in many respects very similar to real experiments. As in experiments, we prepare a sample (which is termed as initialisation of coordinates, which can be either random or ordered), a system consisting of N particles and solve the Newton's equation of motion for this system until the properties of the system no longer change with time (system reaches a state of equilibrium). After the equilibration, actual measurement of interested observables is performed. To measure an observable quantity in a MD simulation, it should be possible to express this observable as a function of the positions and momenta of the particles in the system. For instance, if we intend measure the temperature of the system, it is done so by making use of the equipartition of energy. The average kinetic energy per degree of freedom is

$$\left\langle \frac{1}{2}mv^2 \right\rangle = \frac{1}{2}k_B T \tag{1.16}$$

Hence by calculating the total kinetic energy and dividing it by the number of degrees of freedom the temperature of the system is found.

The fundamental steps involved in the molecular dynamics simulations are as follows:

1. Input parameters that specify the conditions of the run is read in. This includes initial temperature (and pressure), number of particles, density, time step, initial configuration (random or crystal) etc.

2. Initial positions and velocities are selection. As stated before the initial positions can be a random initialisation, if the simulation is done for the liquid or amorphous state or can be a crystal initialisation. Velocities are also chosen randomly, since on equilibrium, it will become Maxwell-Boltzmann distribution.

3. Forces on all the particles are compute. To do so we must be knowing the the kind of interaction particles will have. This is based on the system one is interested in. In our study, for silicon, we use Stillinger-Weber interaction potential, as explained in the previous section.

4. Integrate the newton's equation of motion is find the evolved velocity and the position of the particles.

   Step 3. and 4. form the core of the MD simulation. These steps are repeatedly carried out until we have computed the time evolution of the system for a desired length of time. There are different ways of integration, which are discussed next section.

5. After the system has reached the equilibrium, calculation of desired observables are done. Since we are interested in the average quantities, we do the measurement at certain fixed time period.

Temperature in MD simulation:

The instantaneous temperature T(t) is matched to the desired temperature T by scaling all the velocities with a factor $(T/T(t))^(1/2)$, where

$$T(t) = \frac{1}{k_B} \sum_{i=1}^{N} \frac{m v_{\alpha,i}^2(t)}{N} \tag{1.17}$$

Here, v_α is the α component of the velocity of a given particle. N is the total number of particles.

The above mentioned way of regulating temperature is ad hoc and do not correspond to any known ensemble. Two widely used canonical MD schemes for temperature regulation are Andersen thermostat and Nosé-Hoover thermostat. In our simulation code and in LAMMPS' code [34](which has been used for all the NVT runs in our work), Nosé-Hoover thermostat [14] is used. For the pressure regulation we have used the Andersen's method [7].

Integrating the equation of motion

After calculating the forces between the particles, we need to obtain the evolved position and the velocities, for which we have to integrate the forces. Two integration algorithms, the Verlet algorithm and the Leap-Frog algorithm, are explained below.

Verlet Algorithm: To derive the algorithm we start with a Taylor expansion of the coordinate of a particle, around time t,

$$r(t+\Delta t) = r(t) + v(t)\Delta t + \frac{f(t)}{2m}\Delta t^2 + \frac{\Delta t^3}{3!}\frac{d^3a}{dt^3} + \mathcal{O}(\Delta t^4) \quad (1.18)$$

similarly,

$$r(t-\Delta(t)) = r(t) - v(t)\Delta t + \frac{f(t)}{2m}\Delta t^2 - \frac{\Delta t^3}{3!}\frac{d^3a}{dt^3} + \mathcal{O}(\Delta t^4) \quad (1.19)$$

Summing these two equations and ignoring the higher order terms, we obtain

$$r(t+\Delta t) \approx 2r(t) - r(t-\Delta t) + \frac{f(t)}{m}\Delta t^2 \quad (1.20)$$

Note that this algorithm does not use the velocity to compute the new position. Velocity can be derived from the knowledge of the trajectory, using

$$r(t+\Delta t) - r(t-\Delta t) = 2v(t)\Delta t + \mathcal{O}(\Delta t^3) \tag{1.21}$$

$$v(t) = \frac{r(t+\Delta t) - r(t-\Delta t)}{2\Delta t} + \mathcal{O}(\Delta t^3) \tag{1.22}$$

The estimates of the new position contains an error of order Δt^4 and the velocities are accurate to the order of Δt^2.

After computing the new positions, we may discard the positions at time $t-\Delta t$. The current positions become the old positions and the new positions become the current positions.

Leap-Frog algorithm: This algorithm is similar to the Verlet scheme, but here the velocities are evaluated at half-integer time steps and uses these velocities to compute the new positions. To derive the Leap Frog algorithm from the Verlet scheme, the velocities at the half-integer time steps are defined as follows

$$v(t-\Delta t/2) \equiv \frac{r(t) - r(t-\Delta t)}{\Delta t} \tag{1.23}$$

$$v(t+\Delta t/2) \equiv \frac{r(t+\Delta t) - r(t)}{\Delta t} \tag{1.24}$$

From the latter equation we get the expression for new positions, based on

old positions and velocities:

$$r(t + \Delta t) = r(t) + \Delta t v(t + \Delta t/2) \tag{1.25}$$

From the Verlet algorithm, we get the following expression for the update of the velocities:

$$v(t + \Delta t/2) = v(t - \Delta t/2) + \Delta t \frac{f(t)}{m} \tag{1.26}$$

As the Leap-Frog algorithm is derived from the Verlet algorithm, it gives rise to identical trajectories. However the velocities are not defined at the same time as the positions. As a consequence, kinetic and potential energy are not defined at the same time and hence the total energy cannot be directly calculated. In the velocity Verlet algorithm, we can use the Verlet algorithm in a form that uses positions and velocities computed at equal times. The coordinated are given by

$$r(t + \Delta T) = r(t) + v(t)\Delta t + \frac{f(t)}{2m}\Delta t^2 \tag{1.27}$$

which looks like a Taylor expansion. The update of the velocities is different from the Euler scheme,

$$v(t + \Delta t) = v(t) + \frac{f(t + \Delta t) + f(t)}{2m}\Delta t \tag{1.28}$$

As it can be seen, we can compute the new velocities only after we have computed the new position and forces.

1.3.3 Other calculations and techniques

1. **Radial distribution function, Coordination number and Fifth neighbour distribution** If $g(r)$ is the RDF, then $\rho g(r) d\mathbf{r}$ gives the probability of observing a second particle at a distance $\vec{r}$ and $\vec{r} + d\vec{r}$. Here ρ is the density of the system. To calculate the $g(r)$ in simulation we do the following:

   (a) Choose a value of shell width dr

   (b) Loop over each particle in the system (which will act as a particle at origin). Count all particles that are in a spherical shell at a distance between $\vec{r}$ and $\vec{r} + d\vec{r}$ away from the reference particle. Let this be n.

   (c) Divide this number by $4\pi r^2 \rho dr$. This ensures that $g(r) = 1$ for system with no structure (ideal gas case).

   (d) Divide this number by N, the total number of particles in the system (averaging over different reference particles).

   Hence we get

$$g(r) = \frac{n/N}{4\pi r^2 \rho dr} \tag{1.29}$$

   To compute the coordination number, we have to integrate the radial distribution function between $r = 0$ to $r = r_c$. Here r_c is the distance at which we find the first minima in the $g(r)$. This gives the number of particles in the first coordination shell or the coordination number.

   The fifth neighbour distribution gives the probability of finding the fifth neighbour at a given distance. The calculation is similar to the

one described for $g(r)$, but in here instead of counting all the particles, we count only those particles which are fifth neighbour of the reference particle. For computing this quantity we sort neighbourlist of each particle in ascending order of the distances.

We have used these calculations for recognising the crystallisation of a system and for the structural properties of the system.

2. **Tetrahedrality order parameter** Tetrahedrality order parameter [10] is defined as:

$$q = 1 - \frac{3}{8}\sum_{j=1}^{3}\sum_{k=j+1}^{4}\left(cos(\psi_{jk}) + \frac{1}{3}\right)^2 \tag{1.30}$$

where ψ_{jk} is the angle formed by the lines joining the silicon atom and its nearest neighbours j and k. The order parameter is normalised such that the average q values varies between 0, for the case of ideal gas and 1, for the case of a perfect tetrahedral network. To compute this quantity, as in the case of $g_5(r)$ calculation the neighbour list needs to be sorted first. As a check, we found that for a perfect tetrahedral network (diamond crystal) the order parameter was indeed 1 and for a configuration taken from a high temperature and low density state, the peak value of the order parameter was close to 0.

We have used this calculation for studying the structural properties of the system.

3. **van Hove function** The van Hove function is defined as:

$$G_s(r,t) = \frac{1}{N}\left\langle \sum_{i=1}^{N} \delta\left(r_i(t_2) - r_i(t_1)\right)\right\rangle \tag{1.31}$$

Physically, the van Hove function gives the distribution of particle displacements over the simulated time. To calculate this quantity first we define a bin width dr. Then we calculate the distance $|\vec{r}_i(t_2) - \vec{r}_i(t_1)|$ the particle 'i' has traveled in the time interval $(t_2 - t_1)$. Then we obtain the histogram of distances.

We have used this calculation for the analysis of low temperature liquid, where the dynamics is very slow.

4. **Overlap function** This is defined as

$$Q(t) = \int d\vec{r}\rho(\vec{r},t_0)\rho(\vec{r},t+t_0) \sim \sum_{i=1}^{N} w(\vec{r}_i(t_0) - \vec{r}_i(t+t_0)) \tag{1.32}$$

Here $\rho(\vec{r},t_0)$ is the space-time dependent particle density. The delta function is course grained by defining [24]

$$\begin{aligned} w(r) &= 1 \text{ if } r \leq a \\ &= 0 \text{ otherwise} \end{aligned}$$

The window function, a, treats the particle positions separated due to small amplitude vibrational motion as same. The window function is chosen from RMSD (root mean square displacement) at the short time lengths. From the overlap function we calculate the relaxation time.

Chapter 2

Liquid-liquid critical point in supercooled silicon

It is known that the vapour pressure curve (liquid-gas coexistence line) does not extend forever, but terminates at a point, which is termed as the critical point. A critical point is defined as a second order phase transition, where the second derivative of free energy (the heat capacity and the compressibility) diverges. One of the most exciting visual experience of a critical phenomena is the *critical opalescence* (strong scattering of light when the system is at its critical point). At the critical point, along with the compressibility (and heat capacity) divergence, the correlation length also increases dramatically In fact, when the correlation length of system acquires dimensions of the order of wavelength of light, then we see the strong scattering of light - which is the reason behind the phenomena of critical opalescence. In our work we use the divergence of compressibility as one of the criteria to find the critical point. We find the compressibility from equation of state as well

as from the volume fluctuations.

Equation of state for a system express the state of system under a given set of physical constraints. More specifically, given a temperature, the equation of state (eos) expresses the relation between pressure and density. From the shape of the eos one can get the indication to approach towards a critical point (will be discussed in this section). Construction of equation of state from the MD simulations was the first step we have taken to locate the liquid-liquid critical point in supercooled silicon. After we have obtained the equation of state we have calculated the compressibility. From the inputs we got from these two calculation we could fix the upper bound for the critical temperature. Below the critical point, we know the system will be unstable and it phase separates in two distinct liquid phases, the HDL and the LDL. [Note, the high temperature liquid is also the high density liquid (HDL) and the low temperature liquid is the low density liquid (LDL)]. Hence finding the phase coexistence or the phase separation puts the lower bound to the critical temperature. In summary, to find the critical point we took the following path:

1. Construction of equation of state from MD simulations.

2. Calculation of the compressibility from eos and volume fluctuation.

3. Finding the phase coexistence below the critical temperature.

2.1 Equation of State

In order to obtain the equation of state for the supercooled silicon, we have performed isothermal-isobaric (NPT) molecular dynamics simulation using the Stilling-Weber potential for liquid Silicon. We have taken 512 particles for all the NPT simulations. From the 1000 particles system we have found there is no system size dependence on the equation of state away from the critical point. The simulation protocol is as follows:

1. Choose an Isotherm (fixing of temperature).

2. Choose a set of pressures for the chosen temperature.

3. Initialise the system (random initialisation). Perform the MD simulation at this at the chosen T and P till the system equilibrate. Once the system has reached equilibration perform production MD runs, from which the required data is calculated (Eg., energy, density, g(r), mean square displacement and other observables).

4. Perform the MD simulation simulation with different initial configuration (minimum of three independent samples were simulated at each state point (T,P)).

5. From the equlibrated NPT MD runs, find the average density for each sample and average it over different samples.

The density and pressure so obtained gives us the equation of state. The range of temperature and pressure over which the simulations were carried out were fixed based on the inputs from previous work by Sastry and Angell.

The liquid-liquid transition at zero pressures was shown to be at $1060K$. Hence the temperatures at which we perform simulation should be higher than this temperature. We started with $T = 1543K$. Since the critical point was predicted to be at negative pressures, to start with we performed our simulation between -4.0 GPa and +4 GPa. Since the system shows tendency to crystallise at certain state points, care was taken to recognise the crystallised configuration while calculating the observables. In the following subsection details about the equilibrium criteria and relaxation time is discussed. We find the relaxation time in the LDL is few order of magnitude bigger than the relaxation time in HDL.

2.1.1 Equilibration criteria

In any system (under a given constraint), there is a tendency to evolve towards states in which the properties of the system, such as the total energy, become time independent. When the system reaches such a state, we say the system has reached equilibrium. Even though there will fluctuations in these properties, the mean will not change with time for a equilibrated system. In molecular simulations, we can look at the evolution of energy with time to decide on the equilibration of the system.

Supercooled silicon being a metastable phase is prone to crystallisation. Before we look at the equilibrium of the system at a given state point we make sure that the system is in the liquid state. There are certain properties of the system which distinguishes system which have crystallised from system which is in a liquid state. We have looked at the energy, the mean square

displacement (msd) and the radial distribution function ($g(r)$).

Energy as function of time: As stated before, supercooled silicon is in a metastable state. Usually, the energy of a system in metastable state will be higher than the energy of the stable state, (Crystal). Hence when when the system in supercooled liquid state crystallises, there will be a jump in energy as shown in FIG. 2.1.

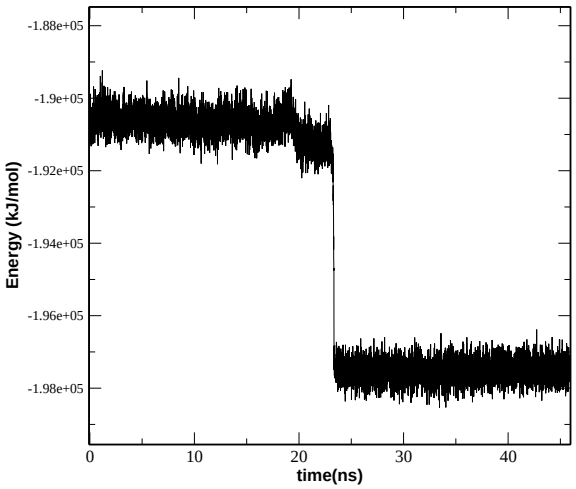

Figure 2.1: Plot of potential energy against MD time step. The jump in the value of potential energy indicate that the system has crystallised (at T = 1158 K and P = -1.88 GPa).

.

Radial distribution function: The radial distribution function or the pair correlation function, denoted as $g(r)$, is related to how particles are packed together. $4\pi r^2 \rho g(r) dr$ gives the number of particles between r and $r + dr$ about a reference particle (ρ being the density of the system). There is a regular arrangement of the atoms in a crystal and hence g(r) peak at regular interval of distance from a reference point in the system. The first minima in the g(r) represents the first coordination shell of the crystal. Similarly, the second minima represents second coordination shell and so on. In case of a liquid, g(r) exhibits peaks only till certain distance, indicating local ordering. At longer distances g(r) dies down to a constant value, indicating equal probability of finding the particles, from a reference point, at these distances. In our work we find for a system which is crystallising, a peak evolves between the second and third peak of the g(r). Figure 2.2 shows the g(r) for a liquid phase, its evolution to a crystal phase and complete crystal phase.

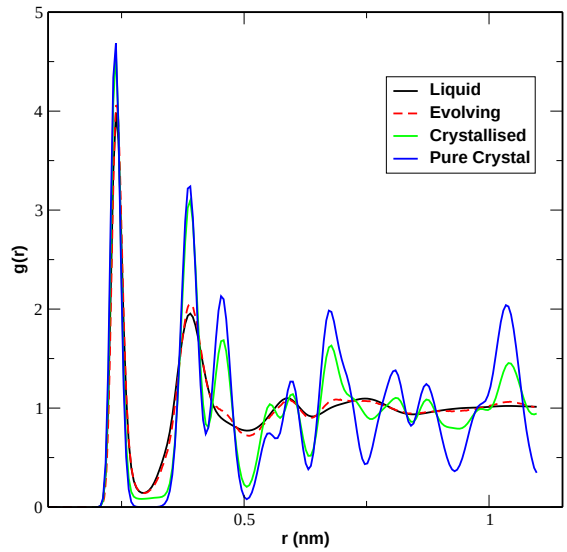

Figure 2.2: Plot of g(r) against distance. An evolution of a small peak is seen between the second and third major peaks, which is an indicator of crystallisation. The green line shows the fully crystallised sample which started from the liquid state and the blue line shows the g(r) for the pure crystal case (at T = 1158 K and P = -1.88 GPa).

.

Mean square displacement: Mean square displacement gives us the displacement of a particle in a system. In the case of liquid, which shows a diffusive behaviour, the MSD should linearly increase with the time (Fig. 2.3).

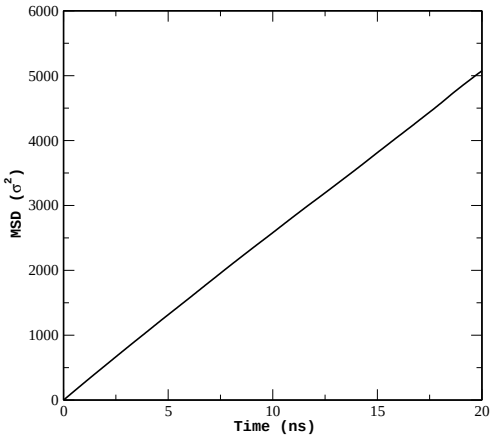

Figure 2.3: Plot of MSD against MD time step for the liquid phase at T = 1259 K and P = 0 GPa. The linear behaviour suggest the system is diffusive.

.

Now, after we have made sure that the system is in the liquid phase, we will address the criterion for equilibrium. One direct and simple way to judge the equilibrium of a system is to look at the energy trend as function of time. If the energy is not fluctuating around a mean value, but showing the trend of going to lower values, that gives a preliminary indication of a system which is either yet to reach equilibrium or aging (wherein the system evolves very slowly and shows no sign of reaching equilibrium). In FIG 2.4 we show one such case. In this case (system at $T = 1158K$ and $P = -1.5GPa$), we have done a simulation for total time around $90ns$. Each color represent simulation time windows of $22.5ns$ (Note that in MD simulation we can

stop and continue the 'experiment' from exactly same point where we had stopped). For each time window we have calculated the MSD which also indicates system is still evolving (FIG. 2.5 - right panel). For an equilibrated system, the slope of the MSD and hence the diffusivity should not change. In this particular case we see diffusivity is changing with the time and hence we conclude system is yet to equilibrate. From the $g(r)$ plot (FIG. 2.5 - left panel), we also observe a small peak evolving after $40ns$ simulation. This, as explained before, is indicating at the crystallisation of the sample (which can be also seen as small jump in energy, in FIG. 2.4, at around $50ns$). This particular case clearly illustrates both the challenges, the slow dynamics and the tendency to crystallise, associated with the study of supercooled silicon.

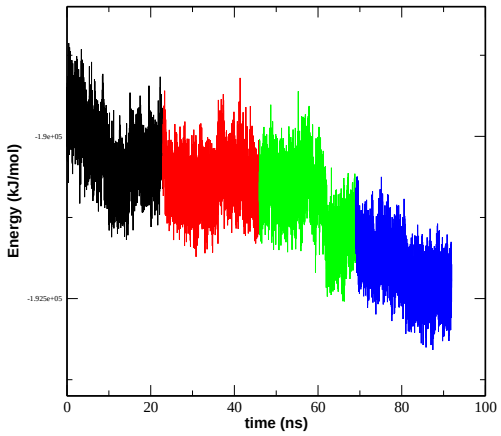

Figure 2.4: Plot of potential energy against MD time step shows that the system is yet to equilibrate (at T = 1158 K and P = -1.5 GPa) even after a very long simulation. Each color represent simulation length of $22.5ns$.

.

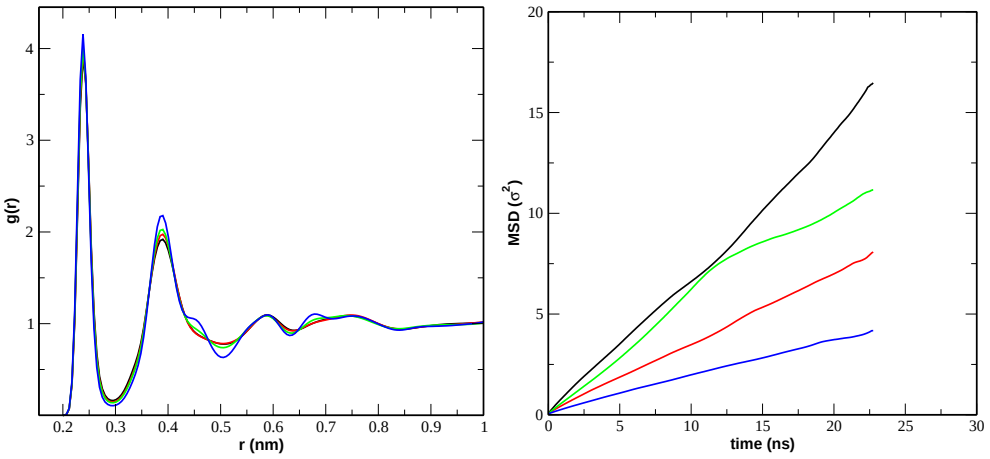

Figure 2.5: Plot of MSD against MD time step (right panel) shows that the system is yet to equilibrate (at T = 1158 K and P = -1.5 GPa). Each colour represents a time window of 22.5ns in the trajectory of total time of 92 ns. As the system evolves the diffusivity is changing, which is indicating that the system has not reached its equilibrium state. In the left panel, a small peak in the $g(r)$ evolving between the second and third peak, indicates that the system is crystallising after 40ns of simulation.

2.1.2 Relaxation times

Relaxation time is defined as the time required for a system to evolve completely (or relax completely) in to a equilibrium state. We have calculated the relaxation time from the density-density correlation function. A density-density correlation function measures the correlation of the fluctuations of the density from its mean values at different positions or at different times. When the densities at different positions or at different times become uncorrelated, this function goes to zero and we tell the system has relaxed completely. We calculate the overlap function, which is a two point correlation function in density to find the relaxation time. Overlap function is defined as

$$Q(t) = \int d\vec{r}\rho(\vec{r}, t_0)\rho(\vec{r}, t + t_0) \sim \sum_{i=1}^{N} w(\vec{r}_i(t_0) - \vec{r}_i(t + t_0)) \qquad (2.1)$$

where $\rho(\vec{r}, t_0)$ etc are space-time dependent particle densities, $w(r) = 1$, if $r \leq a$ and zero otherwise [24]. The window function, a, treats the particle positions separated due to small amplitude vibrational motion as same. The window function a is chosen from RMSD (root mean square displacement) at the short time lengths. Note that the second part of the definition is an approximation which uses only the self-term. The structural relaxation time τ is found by a stretched exponential fit of the long-time decay of Q(t).

The relaxation times calculated from the overlap function is given in the Table 2.1 (for fixed pressure and different temperatures) and 2.2 (for fixed temperature and different pressures).

Temperature(K)	Relaxation time(ns)
1108	0.5×10^{-3}
1082	1.6×10^{-3}
1070	3.6×10^{-3}
1067	4.4×10^{-3}
1062	10.0×10^{-3}
1057	25.0
1052	27.0

Table 2.1: Relaxation time for different temperatures ($P = 0GPa$)

Pressure(GPa)	Relaxation time(ns)
0.76	0.7×10^{-3}
0.38	1.2×10^{-3}
0.00	6.7×10^{-3}
-0.15	0.11
-0.76	23.0

Table 2.2: Relaxation time for different pressures ($T = 1070K$)

The jump in the relaxation time (for $P = 0GPa$) is attributed to the phase transition, which occurs around 1060 K. The dynamics in the LDL phase is very slow as compared to HDL. To obtain equilibrated data in the LDL we need to do tens of nano second simulation which amounts to millions of MD steps (23 ns simulations is around 60 million MD steps for $\Delta t = 0.4fs$) and months of computation time.

To obtain the complete equation of state for the supercooled silicon we have performed MD simulations at nine isotherms. At each isotherm we have simulated at ten or more pressure values. The equation of state is shown in FIG. 2.6. Following are the key observation we make from the equation of state

1. The isotherms between 1510 K and 1133 K are monotonic and continuous. This suggests that for each pressure there is a unique density associated, which means all these isotherms are above critical point.

2. The low temperature isotherms (starting from 1196K) show an intriguing trend: each exhibit an inflection in the region around a density $2.3gcm^3$, which increases in strength as temperature is decreased. The shape and temperature dependence of these inflections are similar to what would occur for isotherms if a critical point were approached from above in temperature.

3. Below certain temperature (1133 K), we find at certain pressures there are jumps in density. This is an indication of phase separation. We confirm the phase separation from the NVT simulation. A van der Waals loop occur when a region of positive slope interrupts the negative slope

of the P-V isotherm. The positive slope corresponds to negative compressibility, a thermodynamically unstable state and hence the liquid phase separates. We find van der Waals loop in this region, confirming the phase separation. In FIG. 2.7 we show our results from the NVT simulation.

4. We observe one more interesting aspect in the equation of state. At positive pressure around $1.5GPa$, the high temperature isotherm cross the other isotherms. Isotherm crossing is also seen at negative pressures (around $-1.5GPa$), but at these state points we need better data equilibration to confirm this behaviour. At zero pressure we find that the density decreases with decrease in temperature.

From the equation of state and from the van der Waals loop we have bound the critical point between two temperature: $1133K$ and $1108K$. Next we calculate the compressibility from equation of state and from the volume fluctuation from the NPT simulation.

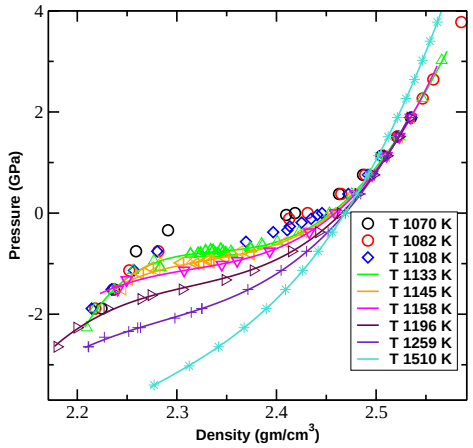

Figure 2.6: Plot of pressure against density -equation of state- for nine different isotherms. The symbols represents the data from NPT simulation. The solid line is the polynomial fit to these data points. The isotherms below $T = 1133K$ are below the critical point and hence a jump in density is observed.

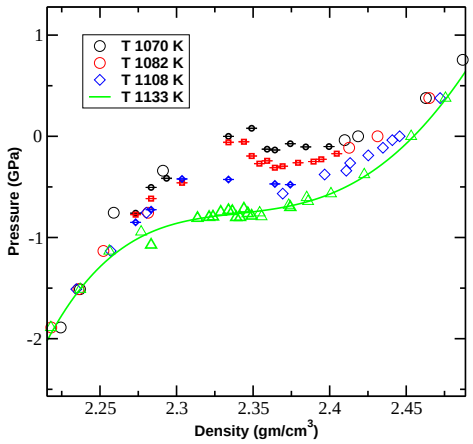

Figure 2.7: Plot of pressure against density for isotherms which are at or below the critical temperature. The light symbols represent the data from NPT simulation. The dark symbols are data from the NVT simulation. The thick line represents the polynomial fit.

2.2 Compressibility

At the critical point, the two phases have equal density and specific entropy, but the second derivative of the Gibbs potential diverges. Compressibility, which is the second derivative of the Gibbs potential (at constant temperature) should diverge. We have calculated compressibility in two different methods. First method is to find the compressibility from the equation of state, using the relation

$$K_T = \frac{1}{\rho}(\frac{\partial \rho}{\partial P})_T \tag{2.2}$$

Before taking the derivative of the equation of state we have done a polynomial fit to the data points obtained from NPT simulation. Second method we have used to find the compressibility is from the volume fluctuation using the relation

$$K_T = \frac{< V^2 > - < V >^2}{< V > k_B T} \tag{2.3}$$

Figure 2.8 shows the compressibility calculated from both the methods. The solid line represents the K_T calculated from eos and the symbols represent the K_T calculated from the volume fluctuations. The compressibility increases with decrease in temperature. At the critical temperature the compressibility diverges. From the equation of state, van der Waals loop and the compressibility calculations we conclude the critical point exists for the supercooled silicon liquid-liquid transition. Even though the current study can't pinpoint at the critical point, our study precisely shows the location of the critical point. The critical temperature is between the $1133K$ and $1108K$, the critical pressure is around $-0.75GPa$ and the critical density is around $2.3gcm^{-3}$.

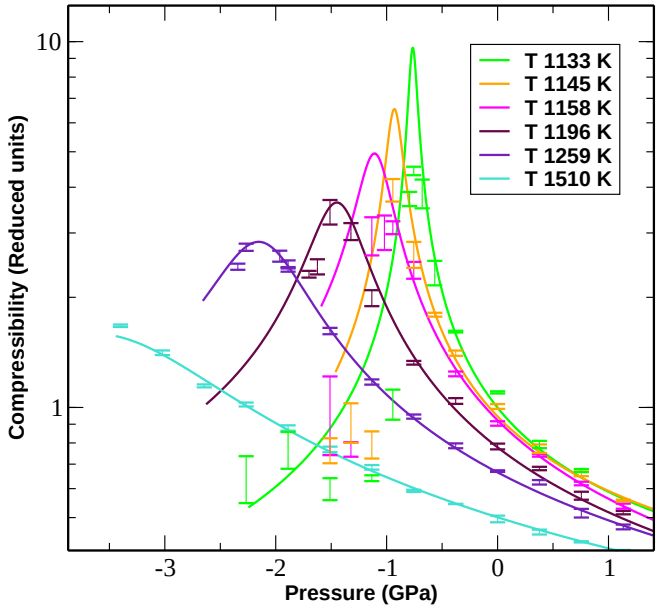

Figure 2.8: Plot of compressibility against pressure for different temperatures. All these isotherms are below the critical point. With the decrease in temperature the compressibility maxima is increases, suggesting approach to the critical point. The thick line represents the compressibility calculated from the equation of state. The symbols represents the compressibility calculated from the volume fluctuations.

Before concluding this chapter we note here few studies which are underway. As it can be seen from the compressibility plot, the values of K_T calculates from the volume fluctuations are not matching with the values calculated from the equation of state. We believe the reason to be a combination of sampling and equilibration of these data point. The compressibility calculated from the equation of state strongly depends on how well we do the polynomial fit. This depends mainly on the data points at the region where we observe the inflection in the eos and data point at tail end of the eos (high negative pressure region). There are two main difficulties in these regions -

Crystallisation and Slow dynamics. The First problem is faced mostly at the inflection region, as we go nearer to the critical point. As it has been already stated, the relaxation time in LDL phase (which is the tail part of equation of state) is of the order of tens of nanoseconds. For the LDL phase we have done parallel tempering simulations in NVT ensemble. We are calculating the compressibility from the pressure fluctuations using hypervirial [9]. Both these studies are in the process of completion and we believe these simulation will better the quality of data points at these regions.

In the next section we discuss some of the properties of supercooled silicon.

Chapter 3

Properties of supercooled silicon

From our study we have found that the two liquids show distinct relaxations times. The HDL equilibrates faster than the LDL. Equilibration is associated with how fast the system explores the phase space to find the minimum energy configuration and hence associated with the dynamics of the system. In this chapter we discuss the results from our diffusivity calculations, which characterises the dynamics in the system. We have obtained the diffusivity from the mean square displacement. The structural properties of both the phases have been analysed by studying the radial distribution function and fifth neighbour distribution. The change in local structure has been studied using the tetrahedrality order parameter. Our study show an interestingly tight knit relation between the structure and the dynamics and a scaling behaviour in temperature.

3.1 Dynamic properties

We characterise the dynamics of the system by the diffusivity calculated from the mean square displacement.

$$D = \lim_{t\to\infty} \frac{1}{6t} < |\vec{r}(t) - \vec{r}(0)|^2 > \tag{3.1}$$

We have calculated the diffusivity at both, below and above the critical point. Below the critical point we see a jump in the diffusivity as the liquid transforms its phase (FIG. 3.1). Above the critical point diffusivity changes continuously. We find there supercooled silicon shows anomalous behaviour in diffusivity as a function of pressure i.e., the diffusivity decreases with decrease in pressure. With the application of pressure the dynamics is becoming faster. The reason behind this, we believe, resides in the local structural arrangement of the atoms. The structural properties that we have calculated shed some light on this aspect.

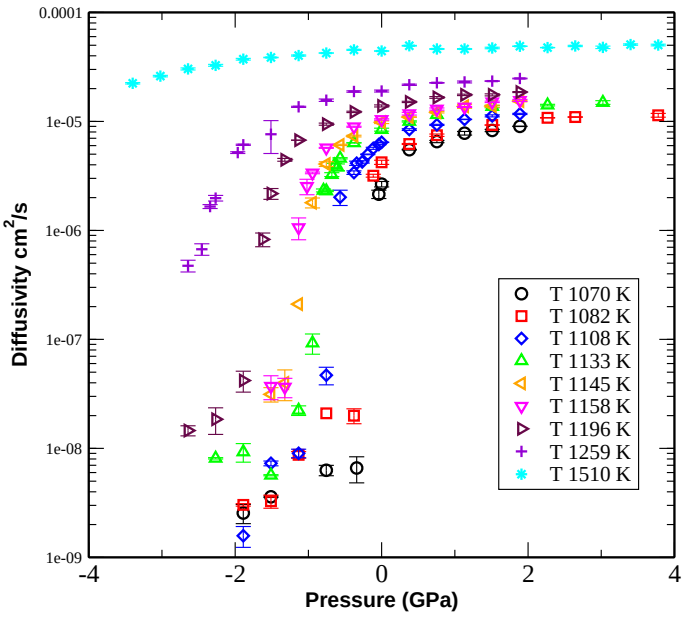

Figure 3.1: Plot of diffusivity against pressure at different temperatures. Diffusivity decreases with decrease in pressure.

3.2 Structural properties

To study the structure of both the phases of supercooled silicon, we have calculated the radial distribution function (RDF) and we have obtained the coordination number (number of particles in the first coordination shell) from the RDF using the relation

$$C_{nn} = \int_0^{r_c} 4\pi r^2 \rho g(r) dr \tag{3.2}$$

where r_c is the distance at first minima of the g(r). We find in our study, $r_c = 2.93\mathring{A}$ for all temperatures and pressure. Coordination number as a function of pressure at different temperatures is shown in the figure 3.2. The coordination number varies from 4.6 to 5.0 for the case HDL which decreases to around 4.2 for the case of LDL. Below the critical point we see a jump in the coordination number and above we have a continuous transition of coordination number. The local structure in both the phases has been analysed by looking at the fifth neighbour distribution and tetrahedrality order parameter.

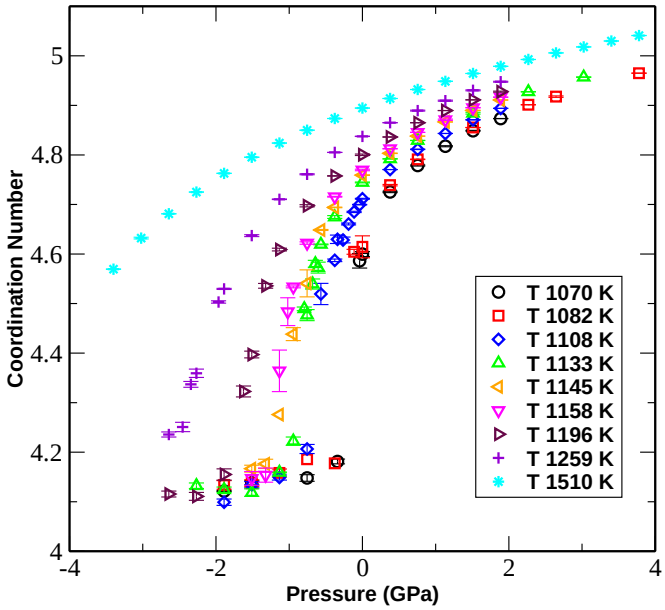

Figure 3.2: Plot of coordination number against pressure at different temperatures. The coordination number for the HDL phase varies from 4.6 to 5. In the LDL phase the coordination number is around 4.2.

Fifth neighbour distribution: The radial distribution function can be decomposed according to the contributions from the successive nearest neighbors. $g_i(r)$'s are defined as sub-RDF's such that

$$g(r) = \sum_{i=1}^{\infty} g_i(r) \tag{3.3}$$

$4\pi r^2 g_i(r)\rho dr$ gives the probability that i^{th} nearest neighbour of reference atom will be found at a distance between r and $r + dr$. We are interested in finding the fifth neighbour distribution, $g_5(r)$. The calculation of $g(r)$ and $g_5(r)$ obtained for isotherms above and below the critical point is shown in FIG. 3.3 and FIG. 3.4 respectively. For the case of HDL we see in the radial distribution function a small peak between the first two major peaks. This feature continues to exist at higher temperature even in case of liquid silicon [6]. This feature can be attributed to the fifth neighbour's presence (see inset of the 3.3 and FIG. 3.4). The fifth neighbour distribution for temperature above the critical point show clearly a smooth developing of a bimodal distribution, which suggests as we go lower in pressure (to LDL), the fifth neighbour moves out of the first coordination shell.

Tetrahedrality Order Parameter: From the $g(r)$ and $g_5(r)$ analysis we have found the number of atoms in the first coordination shell and how they change with transition. The local structure of these atoms is analysed by calculating the tetrahedrality order parameter [10], which is defined as

$$q = 1 - \frac{3}{8} \sum_{j=1}^{3} \sum_{k=j+1}^{4} \left(cos(\psi_{jk}) + \frac{1}{3} \right)^2 \tag{3.4}$$

where ψ_{jk} is the angle formed by the lines joining the silicon atom and its nearest neighbours j and k. This order parameter varies between 0, for the case of ideal gas and 1, for the case of a perfect tetrahedral network. From this order parameter we find how the local arrangement of atoms are in both the phases. FIG. 3.5 shows the distribution of tetrahedrality order parameter calculated at a wide range of temperatures (from LDL to HDL to normal liquid) at zero pressure. We observe at lower temperature, the supercooled liquid is having local tetrahedral structure. As we move to higher temperatures the tetrahedrality decreases. The angle ψ_{jk} is equal to 109.47° for a perfect tetrahedron. It has a value around 102° for the lowest temperature we have measured ($T = 1007K$), which decreases to a value around 90° for the highest HDL temperature we have measured ($T = 1510K$). In case of liquid silicon this angle has been found to be between 60° and 90° [19] (Note that the angle ψ_{jk} was calculated by the inputting the value of q found from simulation in the above definition of tetrahedrality order parameter. We have assumed all ψ_{jk}'s are same for all neighbour atoms. A better estimation is required to be done). We also observe, as we go to higher temperature, a second peak develops at the tail of the order parameter and it grows to become the major peak. This is attributed to the entry of fifth neighbour in to the coordination shell. In FIG. 3.6 we show the tetrahedral order parameter calculated for one temperature at different pressure. It is evident from this figure, as the system undergoes a phase transition from LDL to HDL, the local structure is no longer tetrahedral.

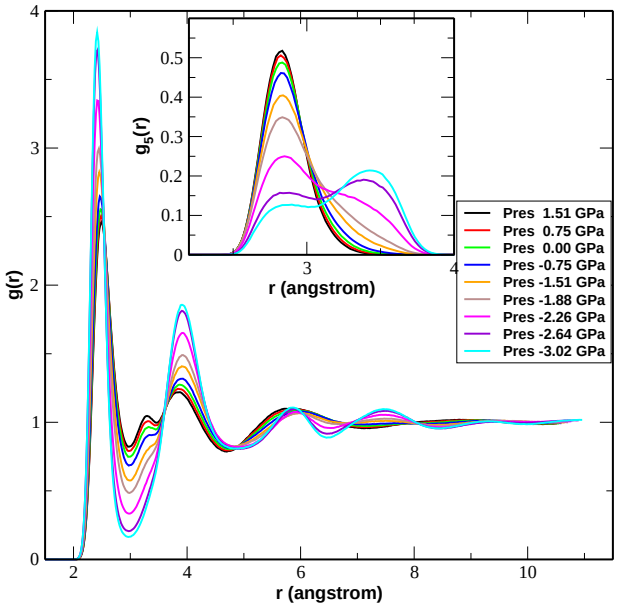

Figure 3.3: Plot of Radial distribution at different pressures at T = 1259 K.

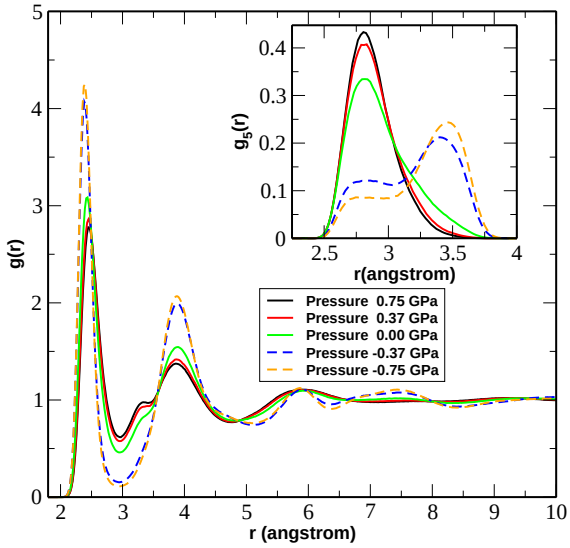

Figure 3.4: Plot of Radial distribution at different pressures at T = 1070 K.

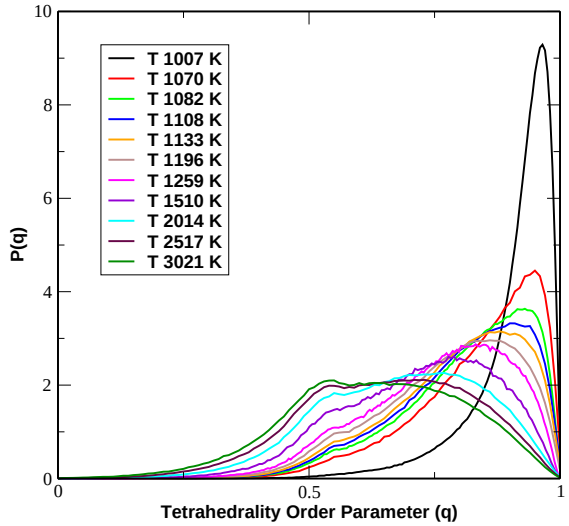

Figure 3.5: Plot of Tetrahedrality order parameter for different temperatures at P = 0 GPa.

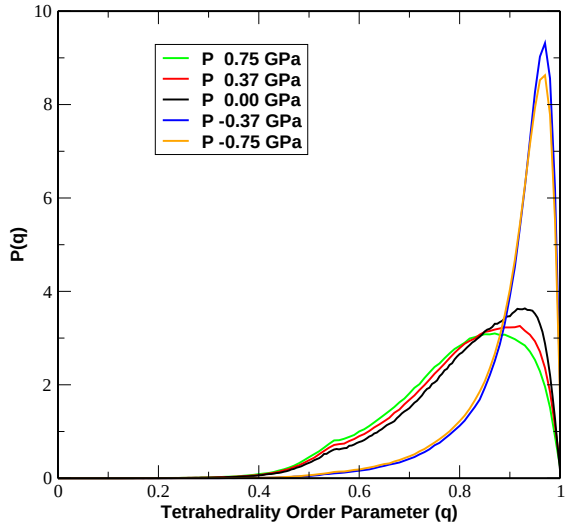

Figure 3.6: Plot of Tetrahedrality order parameter for different pressures at T = 1082 K.

3.3 Structure and Dynamics

In the figure 3.7 we plot the diffusivity as a function of coordination number for different temperatures. We notice that with increase in coordination number the diffusivity also increases. This feature is observed at all the temperatures, above and below the critical point. We notice that when we collapse the data points obtained at different temperatures, all the data points fall in to one single curve (inset of 3.7). There seems to be a scaling behaviour existing in the relation between the dynamics and structure.

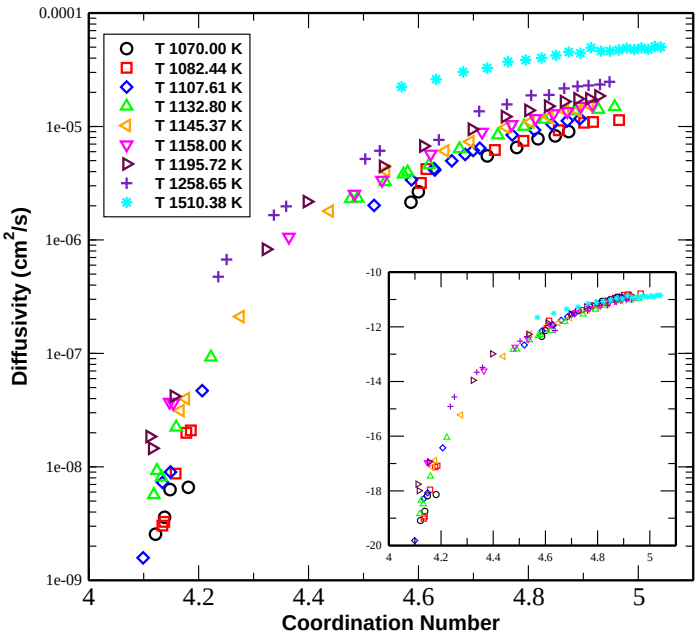

Figure 3.7: Plot of diffusivity against coordination number at different temperatures.

It has been observed in water, the dynamics is influenced by the local

structure [40]. The diffusivity has been directly linked to the topological defects of the tetrahedral network of the water. It has been shown that the defects act as catalysts, providing lower energy pathways between different tetrahedral local arrangement. This seems to be the case even in supercooled silicon. A detailed study needs to be taken up for confirming the reason behind the correlation between the dynamics and the structure.

Chapter 4

Low temperature liquid - Strong liquid

A useful classification scheme for supercooled liquid is given by Angell plot [8]. This is a plot of viscosity against scaled temperature (scaling temperature chosen to be that at which viscosity reaches 10^{13} poise) for a wide variety of supercooled liquids at atmospheric pressure. The Angell plot is shown in FIG. 4.1. In this plot, all those liquids that exhibits the Arrhenius behaviour over the entire temperature spectra (ones on the straight line in FIG. 4.1) are termed as 'Strong' liquids. Those which exhibit marked deviation from the Arrhenius behaviour are termed as 'Fragile' liquids.

In simulations, supportive evidence to the strong liquids has been given in an indirect way [37] [22]. The strong liquid has been observed in experiments [42] to show strong boson peak that persists to temperatures far above glass transition temperature. The boson peak, in simulations, has been identified as a dip in the intermediate scattering function between the short time

dynamics and α-relaxation [17]. But it has been questioned on the basis that the association of intermediate scattering function with boson peak still has no physical basis.

Strong liquids such as SiO_2 and GeO_2, which have tetrahedrally coordinated structure, resist thermal degradation. This is associated to the structural stability, which is reflected as the small heat capacity and thermal expansion coefficient changes that accompany the vitrification of strong liquids. A validation of this has been found in the observation that strong liquid can be made fragile by introducing additional component that disrupt the networked structure [23].

It has been observed [37] that the HDL shows non-Arrhenius behaviour in diffusivity as a function of temperature and hence HDL is a fragile liquid. In our study we also find that the HDL has coordination number greater than four. But the LDL, which has tetrahedral local structure needs a clear evidence of being a strong liquid. Based on the discussions presented in the previous paragraph, the most sensible and unambiguous way to show the LDL to be a strong liquid is by calculating the heat capacity. The challenges associated with this kind of study is two-fold. First, the dynamics in the LDL (or the low temperature phase) is slow and the relaxation times are very large. Second difficulty is the crystallisation. Since the LDL is structurally similar to the crystal phase (both are four coordinated), system often crystallises. The protocol we have followed to counter these difficulties is discussed in the following section.

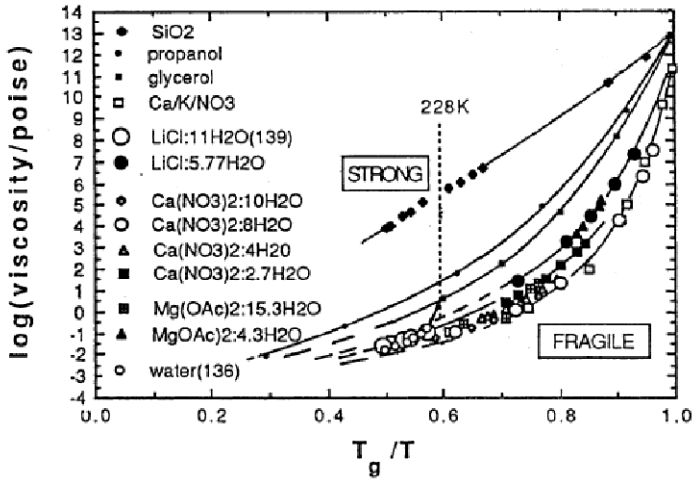

Figure 4.1: Plot of viscosity (in log scale) against the scaled temperature (scaling temperature is the glass transition temperature T_g) [3]

4.1 Approach

At zero pressure, the liquid-liquid transition is found to be at around $1060K$. Above this temperature we have the HDL phase (which from now on will be referred to as the high temperature liquid) and below we find the LDL phase (which from now on will be referred to as the low temperature liquid). We have conducted the simulations at seven temperatures, starting from $1060K$ to $1042K$ and around 60 samples were simulated at each temperature for about $23ns$. We choose the samples which have not crystallised for further MD runs and we have simulated upto $150ns$. Since system evolves very slowly, getting equilibrium state is quite a difficult task. We discuss about this aspect in the following sub-section.

4.1.1 Slow Dynamics - MSD and van Hove function

To exemplify the slow dynamics we show here the MSD and the van Hove function (self-part) calculated at temperatures above and below transition. The van Hove function is defined as:

$$G_s(r,t) = \frac{1}{N}\left\langle \sum_{i=1}^{N} \delta\left(r_i(0) - r_i(t)\right)\right\rangle \tag{4.1}$$

Physically, the van Hove function gives distribution of particle displacement over the simulated time.

For the temperature above the phase transition ($T = 1070K$) and below the transition ($T = 1057K$, and $T = 1052K$) at zero pressures, the MSD and $G_s(r,t)$ are given in FIG. 4.2, 4.3 and 4.4 respectively. We see in the case of

$T = 1070K$, for a relatively short time of $10ns$, the particles, on an average, have traveled more than 20σ, which is reflected in the van Hove function also (FIG. 4.2). But with the phase transition, the particles in the system are moving very slowly. Even after $100ns$, the particles have traveled just around 4σ in the case of $T = 1057K$ (FIG. 4.3). As we go lower in temperature, particles seems to be rarely moving (FIG. 4.4).

Given the difficulties discussed above, it is very likely that the values we intend to calculate will have large error bars. But the overall trend we have obtained indicates at low temperature liquid to be a strong liquid. These results are discussed in next section.

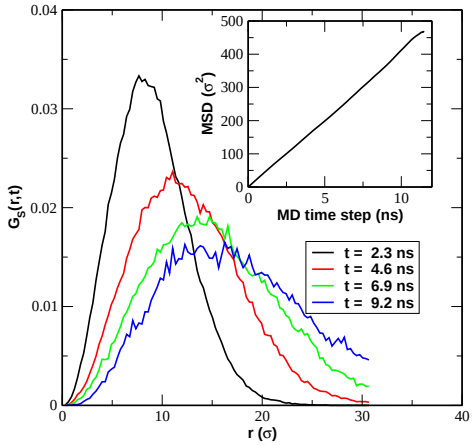

Figure 4.2: Plot of the van Hove function distribution against the MD time function. Inset shows the MSD against the particle displacement ($T = 1070K$ at $P = 0.00GPa$).

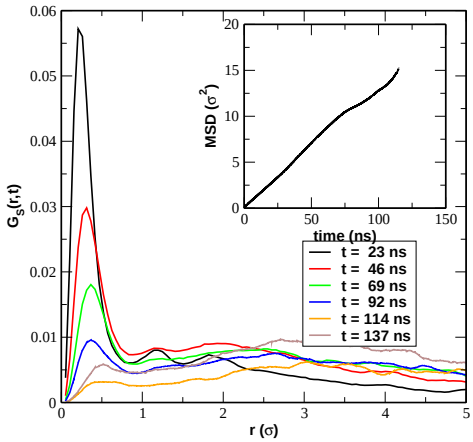

Figure 4.3: Plot of the van Hove function distribution against the MD time function. Inset shows the MSD against the particle displacement ($T = 1057K$ at $P = 0.00GPa$).

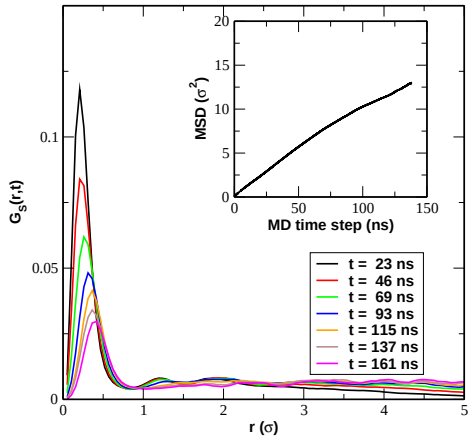

Figure 4.4: Plot of the van Hove function distribution against the MD time function. Inset shows the MSD against the particle displacement ($T = 1052K$ at $P = 0.00GPa$).

4.2 Results

In the Fig. 4.5, the heat capacity (calculated from the fluctuations in potential energy) as a function of temperature is shown. For comparison the heat capacity of crystal is also shown. The data needs to be refined for the low temperature liquid. But it can be seen that there is drastic drop in heat capacity as the liquid makes transition from high temperature to low temperature phase, a signature of strong liquid. In the Fig. 4.6, the diffusivity calculated from the mean square displacement as a function of inverse temperature is shown. Even though better data is required to conclude the Arrhenius behaviour of diffusivity, the current data hints at this behaviour.

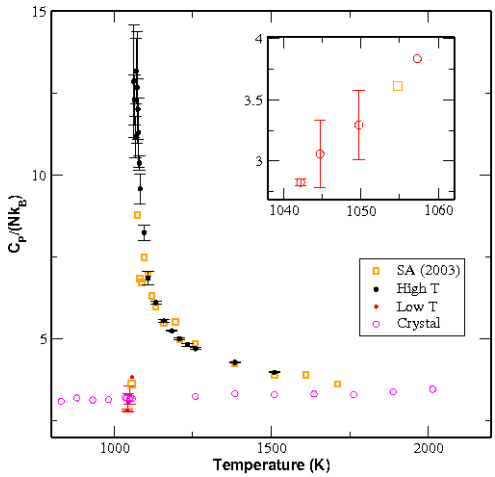

Figure 4.5: Plot of heat capacity against the temperature for high temperature liquid, low temperature liquid and crystal. The orange symbols (with legend SA(2003)) represents the calculation performed by Sastry and Angell. The inset shows the plot for low temperature liquid only.

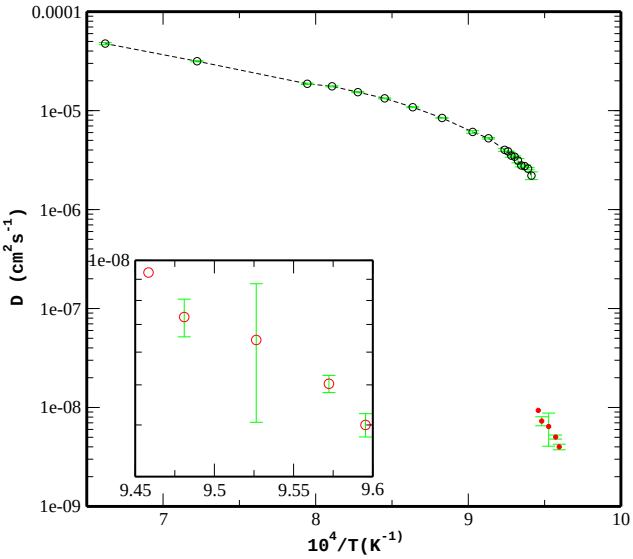

Figure 4.6: Plot of diffusivity against the inverse temperature for high temperature liquid, low temperature liquid. The high temperature liquid (black circles) shows non-Arrhenius behaviour in diffusivity, where are the low temperature(red circles) liquid indicates at Arrhenius behaviour. The inset shows the plot for low temperature liquid only.

4.3 Constrained ensemble Monte Carlo simulation

To improve the quality of the data it is necessary for us to perform simulations longer than the what we have already achieved. Techniques like parallel tempering will not work in the regions of phase transition. But if we can avoid crystallisation in some way, we can carry out the simulations for required amount of time. The approach we have taken to avoid crystallisation is to do a constrained ensemble Monte Carlo simulations. In this approach we try to avoid the crystallisation by finding the cluster size in the system and restricting it from growing above certain threshold. The size of threshold was found (using the method given in [4]) from the existing crystallised runs at each temperature. We define the cluster in the following way.

1. Recognising solid-like particle: To do so first we need to calculate bond angle correlation denoted by G_3(refer [4]). Then we use two conditions to recognize a solid particle.

   (a) G_3 for the particle should be less than certain threshold.

   (b) This particle should have a threshold number of connections with its neighbors.

2. Identifying the cluster: Two solid-like particles belong to the same cluster if the distance between them is less than certain threshold distance.

We apply the constraint as an additional move in the MC simulation (along with the standard displacement and volume change). Every 'm' MC step (we

choose 'm' depending upon how fast the crystallization occurs), we calculate the largest cluster size(n1). If $n1 < n0$ (which is the threshold cluster size), no constraint is applied. If n1 is greater than n0 then we apply the constraint (for which we use a bias potential of the form $k(n-n0)^2$, where k is constant and accept the MC step with a probability $exp(-\beta\Delta w)$, where Δw is the change in bias potential). Initial result from these simulations is shown in the FIG. 4.7 and FIG. 4.8. In this particular case we have taken the threshold n0 to be 50.

The results from this methods needs to be unbiased (applying a constraint to avoid the crystallisation can be seen as putting a bias against growing of critical nucleus) before analysing. This work is still underway.

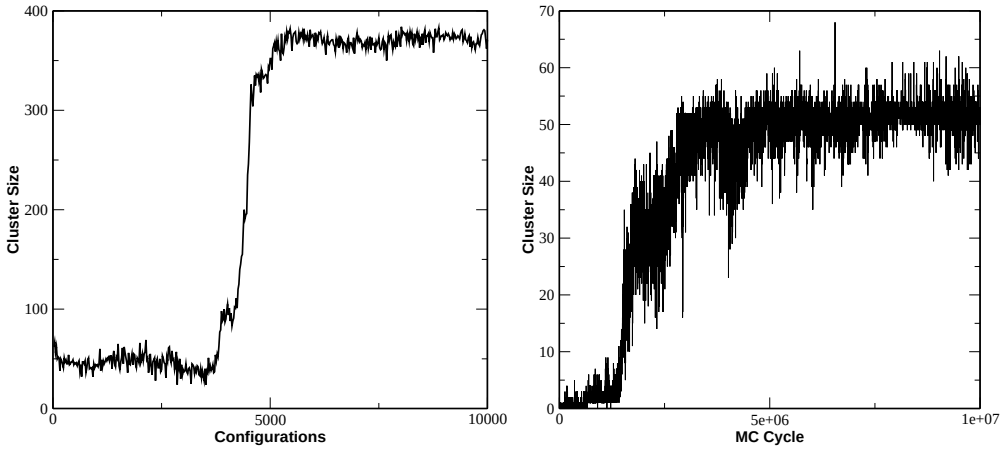

Figure 4.7: In the left panel, the cluster growth is shown from a MD run (each configuration number corresponds to a particular MD step). As it can be seen, the threshold cluster size is around 50 in this case. In the right panel, the cluster growth is shown from constrained MC simulation. Here the cluster growth is restricted to a value around50.

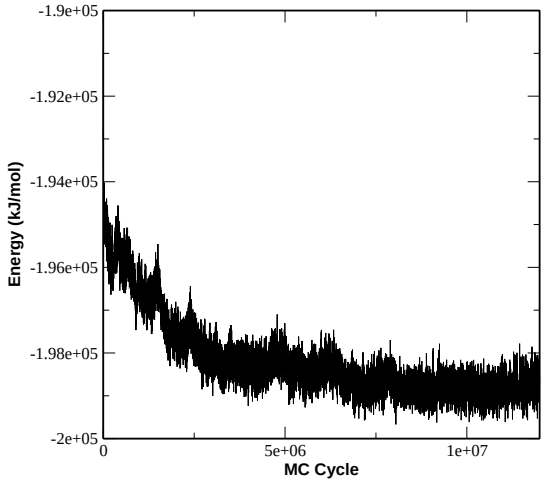

Figure 4.8: Plot of energy against the MC time step from the constrained ensemble simulation.

Chapter 5

Conclusion

5.1 Overview

The principle conclusions of this thesis are:

1. Liquid-liquid phase transition in supercooled silicon (in Stillinger-Weber potential) has a critical end point. The compressibility calculations has given a conclusive evidence for the existence of a liquid-liquid critical point. Our studies have shown that below the critical temperature the supercooled silicon phase separates in to two distinct liquids, HDL and LDL. Above the critical point, a continuous transition is observed. Our studies find that the relaxation time increases by around three orders of magnitude when the liquid undergoes phase transition from HDL to LDL. The reason behind this drastic change is not fully understood, but our studies indicate that the coordination changes is one of the aspects to look at.

2. The approach taken to find the critical point has provided us ample amount of data to fully understand various properties of silicon in its supercooled phase. In this thesis we have focused on structural properties and diffusivity. We have studied, at different temperatures and pressures (both positive and negative), the changes in structure undergone by supercooled liquid. We have found from the radial distribution function calculations, the HDL has a coordination number going up to 5 (as in case of normal liquid phase of silicon) and the LDL has a coordination number around 4 (as in case of crystal phase of silicon). The local structure has been analysed by fifth neighbour distribution and tetrahedrality order parameter. The tetrahedrality order parameter shows that the LDL has local structure similar to that of a crystal (tetrahedral structure) and HDL has a local structure similar to that of a liquid silicon.

   Study of diffusivity of supercooled silicon throws some light on the dynamics of system. Firstly, we find an anomalous behaviour in diffusivity. The diffusivity decreases with decrease in pressure. Secondly we find a strong relation between the diffusivity and coordination number at all the temperatures and pressure we have simulated. We find an interesting scaling in temperature for the relation between diffusivity and coordination number.

3. We have made an attempt to give a decisive evidence for LDL to be a strong liquid. We have calculated the heat capacity and diffusivity at low temperature (zero pressure), where we find the LDL phase. We

find that at the liquid-liquid phase transition from HDL to LDL, there is huge jump in the heat capacity. It is expected for a strong liquid to have a smaller heat capacity value as compared to a fragile liquid. The diffusivity values calculated at different temperatures for the LDL appears to show Arrhenius behaviour which again points at the fact that it is strong liquid.

5.2 Future work

During the course of study of supercooled silicon we have come across certain interesting projects which are stated below:

1. **Coordination number and Diffusivity, Scaling behaviour in temperature :** Lowering the density in supercooled silicon leads to slowing down of the single particle diffusion. A case similar to this is the widely studied liquid - water. It has been shown in water [40], that the decrease in molecular mobility on lowering the density correlates with the presence of defects in the perfect four-coordinated network, whose number decreases on lowering the density. We observed the same behaviour even in supercooled silicon. In water the analysis has been done by using the inherent structure at different densities. This way, the analysis of the bonding as well as of the structure is less ambiguous as thermal vibrations have been subtracted. In [40] the authors analyse the pair-energy distribution and binding energy distribution and find that for a particular coordination number, there exists a minimum in the binding energy. This coordination number is between 4 and 4.5.

Then it is shown that the presence of fifth neighbour weakens bonding and increases the mobility. We intend to study the case of supercooled silicon along the same lines.

Another interesting property, namely, the temperature scaling for the relation between the coordination number and diffusivity will also be a topic of research.

2. **Influence of structure and compressibility on the crystallisation rates:** All along our study of supercooled silicon two issues we had to confront. One is the slow dynamics, which should be taken up as a separate study as explained above. The other one is the crystallisation of samples at certain state points. The question we are interested is whether the crystallisation rates are dependent on local structure or compressibility, i.e., which plays a predominantly bigger role in determining the crystallisation rates. From the current simulation data, we have looked at the raw statistics of number of samples that have crystallized at each state point and sorted them on the basis of compressibility and coordination number. In FIG. 5.1 we show one such data set (for $T = 1133K$). In this figure, the extreme left bar chart shows crystallised run fraction as a function of pressure. Crystallised run fraction is defined as the number samples crystallised divided by the total MD time step. The middle plot shows the compressibility as function of pressure and extreme right, we show the coordination number as a function of pressure. We find even when the coordination number is greater than 4.6 (which is not a tetrahedral structure as in

case of a silicon in crystal phase), the crystallisation rates are high at pressure value $P = -0.75GPa$ (-0.02 in reduced units). Note that at this particular temperature, for pressures greater than $P = -0.75GPa$ none of the samples crystallised.

To quantify the observation, crystal nucleation rates needs to be found. The crystal nucleation rate depends on 1. the probability, P_{crit} that a critical nucleus forms spontaneously and 2. the kinetic factor (κ), which measures the rate at which the critical nuclei subsequently grow. In order to find $P_{crit} = e^{-\frac{\Delta G_{crit}}{K_B T}}$, we need to find the free energy that is required to form a critical nucleus. We have used umbrella sampling Monte Carlo technique [14] for this purpose. Once we compute these, it will be interesting to know how the structure or the compressibility influences the crystal nucleation rates.

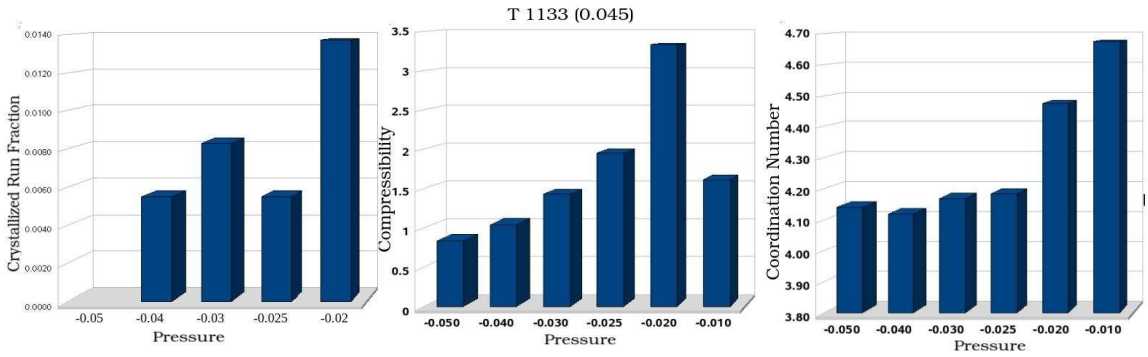

Figure 5.1: Plot showing the crystallised run fraction, compressibility and coordination number as a function of pressure

.

Appendix A

Appendix

A.1 Thermodynamics of phase transitions

A phase transition is an abrupt change in the thermodynamic behaviour which is associated with a discontinuity in free energy. When the first derivatives are discontinuous we have a first order transition and when the first derivatives are continuous but the second derivative is discontinuous we have a second order transition.

First order phase transition

Gibbs free energy is given by

$$dG = -SdT + VdP \tag{A.1}$$

The Volume and the entropy in terms of Gibbs free energy is

$$V = \left(\frac{\partial G}{\partial P}\right)_T \tag{A.2}$$

$$S = \left(\frac{\partial G}{\partial T}\right)_P \tag{A.3}$$

In the first order transition, eg. boiling and freezing of water, the volume and the entropy have different values in the two phases. Because the difference in entropy, crossing the transition line at a fixed temperature make it necessary to absorb or liberate the heat, which is called latent heat.

Second order phase transition

At the critical point, the two phases have equal density and specific entropy, but the second derivative of the Gibbs potential diverges. This is termed as second order phase transition. The second derivatives of the Gibbs potential are the response functions, specific heat and compressibility.

$$Specific\,heat \qquad C_P = -T\left(\frac{\partial S}{\partial T}\right)_P = -T\left(\frac{\partial^2 G}{\partial T^2}\right)_P \tag{A.4}$$

$$Isothermal\,Compressibility \qquad K_T = -\frac{1}{V}\left(\frac{\partial V}{\partial P}\right)_T = -\frac{1}{V}\left(\frac{\partial^2 G}{\partial P^2}\right)_T \tag{A.5}$$

A.2 Van der Waals equation of state

Van der Walls model is gives an approximate equation of state for a fluid system. In an ideal gas scenario, the particle interaction is neglected altogether. Such a treatment results in the ideal gas law,

$$PV = Nk_BT = nRT \tag{A.6}$$

where, P is the total pressure of the system, V is the volume of the system, N is the number of molecules and $n \equiv N/N_A$ is the number of moles in the system, N_A is Avogadro's number, k_B, is the Boltzmann constant and $R \equiv k_B N_A$ is the ideal gas constant.

To describe an interacting gas by means of simple correction to the non-interacting result, one has to take in to account *i*. the finite size of the molecule and *ii*. the attractive force between the molecules.

i. In the ideal gas, the volume of the molecule may be neglected. The equation P = nRT/V means that as we increase the pressure at fixed temperature, the volume decreases without limit. But if we think the molecules to be rigid spheres, there is a minimum volume associated with each molecule (v).

   $V_{min} = N \times v$

   Hence the total volume V in the ideal gas equation is replaced by V - V_{min}. In order that V - V_{min} to be an extensive quantity, V_{min} must be linear in N. Let this proportionality constant be b/N_A. By substituting

this new volume, $(V \rightarrow V - (b/N_A)N$ in the ideal gas equation we get,

$$P = nRT/(V - nb) \tag{A.7}$$

ii. The pressure of the gas is due to the force exerted on to the walls of the container by the molecules of the gas. The attractive forces between these molecules of the gas leads to a decrease in the pressure that gas would exert on the wall of the container. This decrease ΔP has contributions from the decrease in momentum per molecule and from the decrease in the number of hitting to the walls. This contribution is inversely proportional to the square of the specific volume (If we assume a dipole interaction between the molecules, dipole-dipole interaction energy goes as $-1/r^3 \approx -1/v$. Change in the potential energy is given by work $= \int Pdv = -1/v$. Differentiating both sides w.r.t v, we get the pressure $P \approx 1/v^2$). If a is the proportionality constant, we get

$$P = nRT/(V - nb) - an^2/V^2 \tag{A.8}$$

This is the van der Waals equation of state, which is usually written in terms of specific volume and pressure as

$$(p + a/v^2)(v - b) = RT \tag{A.9}$$

The isotherms corresponding to van der Waals equation of motion is shown in the Fig. A.1

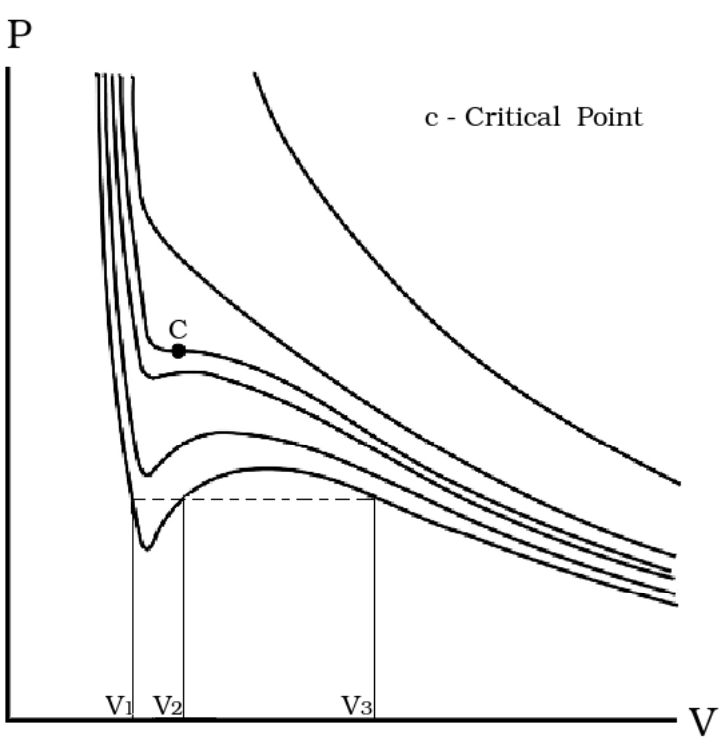

Figure A.1: Schematic plot of pressure against volume showing the equation of state obtained from van der Waals equation.

The pressure at a fixed T is a cubic polynomial in v

$$(v-b)(pv^2-a) = RTv^2 \quad \text{(A.10)}$$

$$pv^3-(bp+RT)v^2-av-ba = 0 \quad \text{(A.11)}$$

There is a region in which the polynomial has three real roots (v_1, v_2 and v_3 in the Fig. A.1). As the T increases, these roots move closer to each other and merge at $T = T_c$, the *critical point*. For $T > T_c$ only one real root remains, while the other two become a complex-conjugate pair. The critical

parameters can be found as follows. At the critical point, the equation of state must be of the form

$$\begin{aligned} (v - v_c)^3 &= 0 \\ v^3 - 3v_c v^2 + 3v_c^2 - v_c^3 &= 0 \end{aligned} \tag{A.12}$$

Comparison with (A.11) gives

$$3v_c = b + \frac{RT_c}{p_c},\ 3V_c^2 = \frac{a}{p_c},\ v_c^3 = \frac{ba}{p_c} \tag{A.13}$$

Solving for T_c, p_c and v_c we get

$$T_c = \frac{8a}{27bR} \tag{A.14}$$

$$p_c = \frac{a}{27b^2} \tag{A.15}$$

$$v_c = 3b \tag{A.16}$$

Reference: Huang, K., 2005, Lectures on Statistical Physics and protein folding, World Scientific.

A.3 Radial distribution function and coordination number

The radial distribution function or the pair correlation function, denoted as $g(r)$, related to how particles are packed together. $4\pi r^2 \rho g(r) dr$ gives the number of particles between r and $r + dr$ about a reference particle.

Consider a system of N particles in a volume V and at a temperature T. The probability that particle 1 is in $d\mathbf{r}_1$ at $\mathbf{r}_1$, a particle 2 is in $d\mathbf{r}_2$ at $\mathbf{r}_2$, etc., is given by

$$P^{(N)}(\mathbf{r}_1, \cdots, \mathbf{r}_N) d\mathbf{r}_1 \cdots \mathbf{r}_N = \frac{e^{-\beta U_N} d\mathbf{r}_1 \cdots \mathbf{r}_N}{Z_N} \tag{A.17}$$

where Z_N is the configuration integral. The probability that particle 1 is in $d\mathbf{r}_1$ at $\mathbf{r}_1$, ..., particle n is in $d\mathbf{r}_n$ at $\mathbf{r}_n$, irrespective of the configuration of remaining $N - n$ particle is obtained by integrating the above equation over the coordinated of particle $n + 1$ through N, which is given by

$$P^{(N)}(\mathbf{r}_1, \cdots, \mathbf{r}_n) = \frac{\int \cdots \int e^{-\beta U_N} d\mathbf{r}_{n+1} \cdots d\mathbf{r}_N}{Z_N} \tag{A.18}$$

Now if we want the probability that any particle is in $d\mathbf{r}_1$ at $\mathbf{r}_1$, and any particle is in $d\mathbf{r}_n$ at $\mathbf{r}_n$, irrespective of the configuration of the rest of the particles, than it is given by

$$\rho^{(n)}(\mathbf{r}_1, \cdots, \mathbf{r}_n) = \frac{N!}{(N-n)!} P^{(n)}(\mathbf{r}_1, \cdots, \mathbf{r}_n) \tag{A.19}$$

The prefactor in the right hand side of equation is due to that fact that, for

first particle we have N ways, for second particle we have $(N-1)$ ways, etc.

For $n = 1$, $\rho^{(1)}(\mathbf{r}_1)d\mathbf{r}_1$ gives the probability of finding one particle at $d\mathbf{r}_1$. For a crystal, this is a periodic function of $\mathbf{r}_1$ and hence there will be a sharp peak at the lattice sites. In case of a fluid, all points within the volume V are equivalent and hence $\rho^{(1)}(\mathbf{r}_1)$ is independent of $\mathbf{r}_1$. Therefore, for a fluid, we can write

$$\frac{1}{V}\int \rho^{(1)}(\mathbf{r}_1)d\mathbf{r}_1 = \rho^{(1)} = \frac{N}{V} = \rho \tag{A.20}$$

A correlation function $g^{(n)}(\mathbf{r}_1, \cdots, \mathbf{r}_n)$ can be defined such that, if the particles were independent of each other, $\rho^{(n)}$ would simply be ρ^n, otherwise

$$\rho^{(n)} = \rho^n g^{(n)}(\mathbf{r}_1, \cdots, \mathbf{r}_n) \tag{A.21}$$

This factor $g^{(n)}$ gives the correlation between the particles. For $n = 2$, we get the pair correlation function $g^{(2)}(\mathbf{r}_1, \mathbf{r}_2)$ or just $g(\mathbf{r})$. From $\rho g(\mathbf{r})d\mathbf{r}$ we get the probability of observing a second particle in $d\mathbf{r}$ given there is a particle at the origin $\mathbf{r}$. If we integrate this term between the limits 0 and a cutoff radius, we get the number particles within that cutoff. If the cutoff is the radius of first coordination shell we get the coordination number.

$$\int_0^{r_c} \rho g(\mathbf{r}) 4\pi r^2 dr = C_{nn} \tag{A.22}$$

Reference: McQuarrie, D. A., 2003, Statistical Mechanics, University science books.

A.4 Mean square displacement and diffusivity

Consider a cloud of diffusing particles starting at time t_0 from the origin and making many individual displacements during the time $t - t_0$. Let $\mathbf{R} = (X, Y, Z)$ be the total displacement of a particle after many individual displacements. $W(X, \tau)$ is a distribution function which defines the probability that after time τ the particle will have traveled a path with a $x-$projection X. W is independent of the choice of origin and only depends on $\tau = t - t_0$. The $Y-$ and $Z-$ component of the displacement can be treated analogously.

Now we can write the balance equation for the number of diffusing particles located in the plane x at time $t + \tau$, if these particles were located in the plane $x - X$ at time t.

$$C(x, t + \tau) = \sum_X C(x - X, t)W(X, \tau) \tag{A.23}$$

where C denotes the concentration of the particles and summation is carried over all values of X. By Taylor expansion, around $X = 0$ and $\tau = 0$, we get

$$C(x, t) + \tau \frac{\partial C}{\partial t} + \cdots = \sum_X \left[C(x, t) - X \frac{\partial C}{\partial x} + \frac{X^2}{2!} \frac{\partial^2 C}{\partial x^2} + \cdots \right] W(X, \tau) \tag{A.24}$$

For small values τ, $W(X, \tau)$ becomes more and more localised around $X = 0$. Hence the terms higher than second order on the right hand side can be omitted. For a constant change in concentration, second derivative and other

higher order terms in the left hand side are removed.

$$C(x,t) + \tau \frac{\partial C}{\partial t} = \sum_X \left[C(x,t) - X \frac{\partial C}{\partial x} \right] W(X,\tau) \tag{A.25}$$

For a normalised distribution $\sum_X W(X,\tau) = 1$. The n^{th} moment of X is given by

$$\sum_X X^n W(X,\tau) = \langle X^n \rangle \tag{A.26}$$

Therefore,

$$\begin{aligned} \sum_X C(x,t) W(X,\tau) &= C(x,t) \\ \sum_X X W(X,\tau) &= \langle X \rangle \\ \sum_X X^2 W(X,\tau) &= \langle X^2 \rangle \end{aligned} \tag{A.27}$$

Substituting the (A.27) in (A.25), we get,

$$\frac{\partial C}{\partial t} = -\frac{\langle X \rangle}{\tau} \frac{\partial C}{\partial x} + \frac{\langle X^2 \rangle}{2\tau} \frac{\partial^2 C}{\partial x^2} \tag{A.28}$$

The first term on the right hand side corresponds to a drift term and the second term to the diffusion term.

In the absence of a driving force, we have $\langle X \rangle = 0$ and the equation (A.28) reduces to Fick's second law, with the diffusion coefficient

$$D_x = \frac{X^2}{2\tau} \tag{A.29}$$

Analogous equations hold for D_y and D_z.

$$D_y = \frac{Y^2}{2\tau};\ D_z = \frac{Z^2}{2\tau} \tag{A.30}$$

In an isotropic medium we get,

$$\left\langle X^2 \right\rangle = \left\langle Y^2 \right\rangle = \left\langle Z^2 \right\rangle = \frac{1}{3}\left\langle R^2 \right\rangle \tag{A.31}$$

Therefore,

$$D = \frac{\langle R^2 \rangle}{6\tau} \tag{A.32}$$

This relation between the MSD and the diffusion coefficient is called the Einstein-Smoluchowski relation.

Reference: Mehrer, H., 2007, Diffusion in solids, Springer.

A.5 Density fluctuation, isothermal compressibility and density-density correlation function

The isothermal compressibility K_T is directly related to the fluctuations in the total number of particles in the system, which in turn is directly related to density- density correlation function. Therefore at $T \rightarrow T_C$, the divergence of K_T is equivalent to the correlation function becoming very long range.

The fluctuation in the total number of particles is given by

$$\begin{aligned}\left\langle (N- < N >)^2 \right\rangle &= < N^2 > - < N >^2 \\ &= \left[\mathscr{Z}^{-1} \sum_{N=0}^{\infty} (N! h^{3N})^{-1} \int d^N\mathbf{r} d^N\mathbf{p} N^2 exp(-\beta U_N + \beta\mu N) \right] \\ &\quad - \left[\mathscr{Z}^{-1} \sum_{N=0}^{\infty} (N! h^{3N})^{-1} \int d^N\mathbf{r} d^N\mathbf{p} N exp(-\beta U_N + \beta\mu N) \right]^2 \end{aligned} \tag{A.33}$$

Here $\mathscr{Z}$ is the grand partition function. The above equation can be written as

$$\left\langle (N- < N >)^2 \right\rangle = (kT)^2 \left(\frac{\partial^2 ln\mathscr{Z}}{\partial\mu^2} \right)_{T,V} \tag{A.34}$$

Since, $PV/kT = ln\mathscr{Z}$, we can rewrite the equation (A.34) as

$$\begin{aligned}\left\langle (N- < N >)^2 \right\rangle &= (kT)^2 \left(\frac{\partial^2 ln(PV/kT)}{\partial\mu^2} \right)_{T,V} \\ &= kTV \left(\frac{\partial^2 P}{\partial\mu^2} \right)_{T,V} \end{aligned} \tag{A.35}$$

Now

$$\left(\frac{\partial P}{\partial \mu}\right)_{T,V} = \frac{\langle N \rangle}{V} = n \tag{A.36}$$

Hence, (A.35) becomes

$$\begin{aligned} \left\langle (N - < N >)^2 \right\rangle &= kTV \left(\frac{\partial (\langle N \rangle / V}{\partial \mu}\right)_{T,V} \\ &= -\frac{\langle N \rangle kTV}{V^2} \left(\frac{\partial V}{\partial \mu}\right)_{T,N} \end{aligned} \tag{A.37}$$

The isothermal compressibility is defined as

$$\begin{aligned} K_T &= -\frac{1}{V} \left(\frac{\partial V}{\partial P}\right)_{T,N} \\ &= -\frac{1}{\langle N \rangle} \left(\frac{\partial V}{\partial \mu}\right)_{T,N} \end{aligned} \tag{A.38}$$

From (A.37) and (A.38) we get the relation between compressibility and the density fluctuations.

$$K_T = \frac{\left\langle (N - < N >)^2 \right\rangle}{\langle N \rangle^2 kT} V \tag{A.39}$$

The density-density correlation function $G(\mathbf{r}, \mathbf{r}')$ measures the correlations of the fluctuations of the density from its average value,

$$G(\mathbf{r}, \mathbf{r}') \equiv \langle \{ n(\mathbf{r}) - < n(\mathbf{r}) > \} \{ n(\mathbf{r}') - < n(\mathbf{r}') > \} \rangle \tag{A.40}$$

where $< n(\mathbf{r}) n(\mathbf{r}') >$ is the probability of finding a particle at the position $\mathbf{r}$ if we know that there is a particle at the position $\mathbf{r}'$.

To relate the compressibility to the density-density correlation function

$G(\mathbf{r}, \mathbf{r}')$, note that,

$$\left\langle (N - < N >)^2 \right\rangle = \left\langle \int d\mathbf{r} \left\{ n(\mathbf{r}) - < n(\mathbf{r} > \right\} \int d\mathbf{r}' \left\{ n(\mathbf{r}') - < n(\mathbf{r}' > \right\} \right\rangle \tag{A.41}$$

Using the definition of $G(\mathbf{r}, \mathbf{r}')$ from (A.40) in (A.41), we obtain

$$\left\langle (N - < N >)^2 \right\rangle = \int d\mathbf{r} \int d\mathbf{r}' G(\mathbf{r}, \mathbf{r}') \tag{A.42}$$

For a spatially uniform system, we can write $G(\mathbf{r}, \mathbf{r}') \rightarrow G(\mathbf{r} - \mathbf{r}')$ and $G(\mathbf{r} - \mathbf{r}')$ $= < n(\mathbf{r}) n(\mathbf{r}') > - n^2$. Hence equation (A.42) can rewritten as

$$\left\langle (N - < N >)^2 \right\rangle = \int d\mathbf{r}'' G(\mathbf{r}'') \tag{A.43}$$

From equations (A.39) and (A.43) we see that the three phenomena, increase in the density fluctuations, increase in the compressibility and increase in the range of the density- density correlation function, observed near the critical point are all interrelated phenomena.

Reference: Stanley, H. E., 1971, Introduction to phase transitions and critical phenomena, Oxford university press.

Bibliography

[1] Aasland, S. & McMillan, P. F. 1994 Density-driven liquid-liquid phase separation in the system $AI_2O_3 - Y_2O_3$ *Nature* **369**, 633–636.

[2] Akahama, Y., Utsumi, W., Endo, S., Kikegawa, T., Iwasaki, H., Shimomura, O., Yagi, T. & Akimoto, S. 1987 Melting curve of black phosphorous *Physics Letters A* **122**, 129–131.

[3] Angell, C. A. 2002 Liquid fragility and the glass transition in water and aqueous solutions *Chem. Rev.* **102**, 2627–2650.

[4] Auer, S. F. 2002 Quantitative prediction of crystal nucleation rates for spherical colloids: A computational study *Thesis* .

[5] Ballone, P. & Jones, R. O. 2004 A reactive force field simulation of liquid-liquid phase transitions in phosphorus *J. Chem. Phys.* **121**, 8147–8157.

[6] Broughton, J. Q. & Li, X. P. 1987 Phase diagram of silicon by molecular dynamics *Phys. Rev. B.* **35**, 9120–9127.

[7] Brown, D. & Clarke, J. H. R. 1984 A comparison of constant energy, constant temperature and constant pressure ensembles in molecular dynamics simulations of atomic liquids *Molecular Physics* **51**, 1243–1252.

[8] Debenedetti, P. G. 1996 Metastable liquids *Princeton university press* .

[9] Ellegaard, N. L. 2006 Two body sums for the sw potential *Unpublished* .

[10] Errington, J. R. & Debenedetti, P. G. 2001 Relationship between structural order and the anomalies of liquid water *Nature* **409**, 318–321.

[11] Franzese, G., Malescio, G., Skibinsky, A., Buldyrev, S. V. & Stanley, H. E. 2001 Generic mechanism for generating a liquid-liquid phase transition *Nature* **409**, 692–695.

[12] Franzese, G., Malescio, G., Skibinsky, A., Buldyrev, S. V. & Stanley, H. E. 2002 Metastable liquid-liquid phase transition in a single-component system with only one crystal phase and no density anomaly *Phys. Rev. E* **66(5)**, 051206–+.

[13] Franzese, G., Marqués, M. I. & Eugene Stanley, H. 2003 Intramolecular coupling as a mechanism for a liquid-liquid phase transition *Phys. Rev. E* **67(1)**, 011103.

[14] Frenkel, D. & Smit, B. 2002 Understanding molecular simulation, 2nd Ed. *Academic press* .

[15] Ganesh, P. & Widom, M. 2009 Liquid-Liquid Transition in Supercooled Silicon Determined by First-Principles Simulation *Phys. Rev. Lett.* **102(7)**, 075701.

[16] Glosli, J. N. & Ree, F. H. 1999 Liquid-liquid phase transformation in carbon *Phys. Rev. Lett.* **82(23)**, 4659–4662.

[17] Horbach, J. & Kob, W. 1999 Static and dynamic properties of a viscous silica melt *Phys. Rev. B* **60(5)**, 3169–3181.

[18] Štich, I., Car, R. & Parrinello, M. 1989 Bonding and disorder in liquid silicon *Phys. Rev. Lett.* **63(20)**, 2240–2243.

[19] Ishimaru, M., Yoshida, K., Kumamoto, T. & Motooka, T. 1996 Molecular-dynamics study on atomistic structures of liquid silicon *Phys. Rev. B* **54**, 4638–4641.

[20] Jakse, N., Kadiri, Y. & Bretonnet, J.-L. 2000 Structural properties of supercooled liquid silicon by molecular dynamics *Phys. Rev. B* **61**, 14287–14290.

[21] Jakse, N. & Pasturel, A. 2007 Liquid-Liquid Phase Transformation in Silicon: Evidence from First-Principles Molecular Dynamics Simulations *Phys. Rev. Lett.* **99(20)**, 205702.

[22] Jakse, N. & Pasturel, A. 2008 Dynamic aspects of the liquid-liquid phase transformation in silicon *J. Chem. Phys.* **129(10)**, 104503.

[23] Jeong, Y. H., Nagel, S. R. & Bhattacharya, S. 1986 Ultrasonic investigation of the glass transition in glycerol *Phys. Rev. A* **34(1)**, 602–608.

[24] Karmakar, S., Dasgupta, C. & Sastry, S. 2009 Growing length and time scales in glass-forming liquids *Proceedings of the National Academy of Science* **106**, 3675–3679.

[25] Katayama, Y., Mizutani, T., Utsumi, W., Shimomura, O., Yamakata, M. & Funakoshi, K.-I. 2000 A first-order liquid-liquid phase transition in phosphorus *Nature* **403**, 170–173.

[26] Kieffer, J. & Angell, C. A. 1989 Structural incompatibilities and liquid-liquid phase separation in molten binary silicates: A computer simulation *J. Chem. Phys.* **90**, 4982–4991.

[27] Kurita, R., Murata, K.-I. & Tanaka, H. 2008 Control of fluidity and miscibility of a binary liquid mixture by the liquid-liquid transition *Nature Materials* **7**, 647–652.

[28] Kurita, R. & Tanaka, H. 2004 Critical-Like Phenomena Associated with Liquid-Liquid Transition in a Molecular Liquid *Science* **306**, 845–848.

[29] Makhov, D. V. & Lewis, L. J. 2003 Isotherms for the liquid-gas phase transition in silicon from npt monte carlo simulations *Phys. Rev. B* **67(15)**, 153202.

[30] Mishima, O. 2000 Liquid-Liquid Critical Point in Heavy Water *Phys. Rev. Lett.* **85**, 334–336.

[31] Mishima, O. & Stanley, H. E. 1998 Decompression-induced melting of ice IV and the liquid-liquid transition in water *Nature* **392**, 164–168.

[32] Monaco, G., Falconi, S., Crichton, W. A. & Mezouar, M. 2003 Nature of the First-Order Phase Transition in Fluid Phosphorus at High Temperature and Pressure *Physical Review Letters* **90(25)**, 255701–+.

[33] Morishita, T. 2001 Liquid-liquid phase transitions of phosphorus via constant-pressure first-principles molecular dynamics simulations *Phys. Rev. Lett.* **87(10)**, 105701.

[34] Plimpton, S. 1995 Fast parallel algorithms for short-range molecular dynamics *J. Comput. Phys.* **117(1)**, 1–19.

[35] Poole, P. H., Sciortino, F., Essmann, U. & Stanley, H. E. 1992 Phase behaviour of metastable water *Nature* **360**, 324–328.

[36] Saika-Voivod, I., Sciortino, F. & Poole, P. H. 2000 Computer simulations of liquid silica: Equation of state and liquid˘liquid phase transition *Phys. Rev. E* **63(1)**, 011202.

[37] Sastry, S. & Austen Angell, C. 2003 Liquid-liquid phase transition in supercooled silicon *Nature Materials* **2**, 739–743.

[38] Sastry, S., Debenedetti, P. G., Sciortino, F. & Stanley, H. E. 1996 Singularity-free interpretation of the thermodynamics of supercooled water *Phys. Rev. E* **53(6)**, 6144–6154.

[39] Scandolo, S. 2003 Liquid-liquid phase transition in compressed hydrogen from first-principles simulations *Proceedings of the National Academy of Science* **100**, 3051–3053.

[40] Sciortino, F., Geiger, A. & Stanley, H. E. 1992 Network defects and molecular mobility in liquid water *J. Chem. Phys.* **96**, 3857–3865.

[41] Skibinsky, A., Buldyrev, S. V., Franzese, G., Malescio, G. & Stanley, H. E. 2004 Liquid-liquid phase transitions for soft-core attractive potentials *Phys. Rev. E* **69(6)**, 061206.

[42] Sokolov, A. P., Rössler, E., Kisliuk, A. & Quitmann, D. 1993 Dynamics of strong and fragile glass formers: Differences and correlation with low-temperature properties *Phys. Rev. Lett.* **71(13)**, 2062–2065.

[43] Speedy, R. J. & Angell, C. A. 1976 Isothermal compressibility of supercooled water and evidence for a thermodynamic singularity at $-45\mathrm{deg}C$ *J. Chem. Phys.* **65**, 851–858.

[44] Stillinger, F. H. & Weber, T. A. 1985 Computer simulation of local order in condensed phases of silicon *Phys. Rev. B* **31(8)**, 5262–5271.

[45] Tanaka, H., Kurita, R. & Mataki, H. 2004 Liquid-Liquid Transition in the Molecular Liquid Triphenyl Phosphite *Phys. Rev. Lett.* **92(2)**, 025701.

[46] Tanaka, H., Kurita, R. & Mataki, H. 2004 Liquid-liquid transition in the molecular liquid triphenyl phosphite *Phys. Rev. Lett.* **92(2)**, 025701.

[47] Tarazona, Y. R. P. 1998 Density functional theory and the asymptotic high density expansion of the free energy of classical solids and fluids *Molecular Physics* **95**, 141–150.